*Economic Geology,* v. 102, pp. 611–631

# The LaRonde Penna Au-Rich Volcanogenic Massive Sulfide Deposit, Abitibi Greenstone Belt, Quebec: Part II. Lithogeochemistry and Paleotectonic Setting*

P. Mercier-Langevin,†

*Geological Survey of Canada, 490 rue de la Couronne, Québec, QC G1K 9A9, Canada, and Institut national de la recherche scientifique–Centre Eau, Terre et Environnement, 490 rue de la Couronne, Québec, QC G1K 9A9, Canada*

B. Dubé,

*Geological Survey of Canada, 490 rue de la Couronne, Quebec, Canada G1K 9A9*

M. D. Hannington, **

*Geological Survey of Canada, 601 Booth Street, Ottawa, Ontario K1A 0E8, Canada*

M. Richer-Laflèche,

*INRS-ETE, 490 rue de la Couronne, Quebec, Canada G1K 9A9*

and G. Gosselin

*Agnico-Eagle Mines Ltd, Exploration Division, Val-d'Or, Quebec, Canada J9P 4N9*

## Abstract

The Au-rich massive to semimassive sulfide lenses of the LaRonde Penna deposit (58.8 Mt at 4.31 g/t Au) are stacked in a steeply dipping, southward-facing homoclinal volcanic sequence forming a continuous, differentiated volcanic succession composed of two main formations: the ca. 2700 Ma Hébécourt Formation and the 2701 to 2698 Ma Bousquet Formation, which corresponds to the uppermost segment of the Blake River Group. The Hébécourt Formation is composed of regionally extensive LREE-depleted ($[La/Sm]_N$ ~0.9) tholeiitic, basaltic to andesitic, massive to pillowed flows that formed a submarine stratum on which the Bousquet Formation was emplaced. The Bousquet Formation is further divided into a lower member and an upper member. The lower member of the Bousquet Formation is composed of feldspar and quartz-phyric tholeiitic felsic (Zr/Y ~3.4, $Zr/TiO_2$ ~860) sills and extensive effusive and volcaniclastic mafic to intermediate and tholeiitic to transitional rocks. The upper member is mainly characterized by submarine, coalesced dacitic to rhyodacitic autoclastic flows that are cut and/or covered by rhyodacitic and rhyolitic domes and/or partly extrusive cryptodomes and by intermediate to mafic sills and dikes.

Mafic to intermediate and tholeiitic to transitional (Zr/Y ~2.3–5) rocks of the Bousquet Formation are characterized by a low $Zr/TiO_2$ ratio (<60), moderately enriched chondrite-normalized LREE and MREE ($[La/Sm]_N$ ~2.2–2.7) patterns, flat HREE ($[Gd/Lu]_N$ ~1.2–2) patterns, and negative Nb, Ta, Zr, and Hf anomalies. Felsic transitional to calc-alkaline (Zr/Y ~5–8) rocks of the upper member of the Bousquet Formation are characterized by a moderate $Zr/TiO_2$ ratio (~250–615), high incompatible element contents, LREE-enriched patterns ($[La/Sm]_N$ ~3.2–6.6), flat HREE patterns ($[Gd/Lu]_N$ ~1–1.4), pronounced negative Nb, Ta, and Ti anomalies, and positive Zr and Hf anomalies. The Nd isotope signature of six separate LaRonde Penna deposit host units ($\varepsilon_{Nd}$ ~3–3.4) suggests that they were generated by partial melting of depleted upper mantle and/or juvenile material (mafic crust) or by a combination of those two processes. The sequence is interpreted to reflect the progression from diapirism of depleted upper mantle associated with underplating by mafic-ultramafic magma and assimilation and magmatic differentiation (assimilation-fractional crystallization) at midcrustal levels in subsidiary magmatic chambers within a ca. 2721 Ma, relatively thick, juvenile or immature mafic ± felsic arc–back-arc crust in an intermediate setting between back-arc basin and volcanic-arc environments. This setting, compatible with the inferred geodynamic setting for the southern Abitibi belt, could be responsible, at least in part, for the Au enrichment of the volcanic massive sulfide (VMS) deposits of the Doyon-Bousquet-LaRonde mining camp.

This study shows that Archean HREE-depleted and high Th, transitional to calc-alkaline dacite, rhyodacite, and rhyolite, referred to as FI and FII type, such as those associated with the LaRonde Penna deposit, can be important hosts for VMS and Au-rich VMS and may be as prospective as the tholeiitic or FIII-type rhyolite-bearing sequences.

† Corresponding author: e-mail, pmercier@nrcan.gc.ca
* Geological Survey of Canada contribution 20060375
** Present address: University of Ottawa, 140 Louis Pasteur, Ottawa, Ontario, Canada K1N 6N5.

## Introduction

The LaRonde Penna Au-rich volcanogenic massive sulfide (VMS) deposit (58.8 Mt at 4.31 g/t Au, 2.17% Zn, 0.33% Cu, and 45 g/t Ag, for about 8.1 Moz of Au) is located in the eastern part of the Archean Blake River Group of the southern Abitibi greenstone belt. The Au-Zn-Cu-Ag-Pb massive to semimassive ore lenses were formed on different stratigraphic horizons, in part, by subsea-floor replacement of felsic flow breccia and mafic to intermediate sills and, in part, by exhalative activity during a single protracted synvolcanic hydrothermal event (Dubé et al., 2004, 2007; Mercier-Langevin et al., 2007a).

The LaRonde Penna deposit and the other Au-rich VMS deposits of the camp are closely spatially and temporally related to felsic volcanism (Mercier-Langevin et al., 2007b), as is common for other VMS deposits of the Superior province (Franklin et al., 1981). However, the geochemistry of the VMS-bearing felsic rocks can vary significantly from one district to another, reflecting a different geodynamic setting and magmatic evolution (e.g., Lesher et al., 1986; Barrie et al., 1993; Yang and Scott, 2003; Hart et al., 2004). These variations are also reflected in the compositions of the ores (e.g., Franklin et al., 1981; Lydon, 1988), and some studies suggest that the trace element content of the felsic rocks can be correlated to the base metal contents of the associated deposits (e.g., Lesher et al., 1986; Barrie et al., 1993; Barrett and MacLean, 1994; Lentz, 1998; Yang and Scott, 2003; Hart et al., 2004). A direct magmatic contribution of volatiles and metals to the hydrothermal system is also commonly proposed to explain the metal contents (e.g., Urabe, 1987; Sawkins, 1990; Hannington et al., 2005). This is especially the case for some Au-rich VMS deposits (Sillitoe et al., 1996; Hannington et al., 1999).

Volcanogenic massive sulfide deposits contain variable amounts of Au (Large, 1992; Hannington et al., 1999), but there is a distinct provinciality of Au-rich VMS deposits that indicates a possible source-rock control (cf. Huston, 2000) and specific geodynamic and petrogenetic conditions that may be favorable for Au enrichment (e.g., Kerr and Gibson, 1993). The well-preserved Archean mafic to felsic volcanic sequence in the Doyon-Bousquet-LaRonde mining camp represents an opportunity to examine the possible association between geodynamic setting, magmatism, and metallogenesis of Au-rich VMS lenses.

This paper documents the primary geochemical features of the volcanic units that host the LaRonde Penna deposit with particular emphasis on the felsic units of the upper member of the Bousquet Formation. The relationship between host rocks, petrogenesis, and ore signatures is examined to test the link between metal content and paleotectonic setting of the VMS deposits and possible applications to exploration strategies.

## Geologic Setting

Lafrance et al. (2003a, b) divided the eastern segment of the Blake River Group in the Doyon-Bousquet-LaRonde mining camp into two different formations: the Hébécourt and the Bousquet Formations. The Hébécourt Formation is mainly composed of tholeiitic mafic rocks (basaltic flows and gabbro sills) overlain by the Bousquet Formation. The latter is further divided into the lower member and the upper member. The lower member is composed of tholeiitic to transitional, mafic to felsic rocks, whereas the upper member is dominated by transitional to calc-alkaline, intermediate to felsic rocks (Lafrance et al., 2003a; Mercier-Langevin et al., 2007a). Overall, the Bousquet Formation is characterized by a gradual evolution from tholeiitic at the base (north) to calc-alkaline at the top (south), defining a continuous magmatic trend rather than a bimodal volcanic sequence, as in the Noranda Volcanic Complex located in the central part of the Blake River Group (Gélinas and Ludden, 1984; Gélinas et al., 1984). The units of the lower member of the Bousquet Formation are laterally extensive, whereas the felsic units of the upper member are laterally restricted, coalesced flows (Stone, 1990; Lafrance et al., 2003a). The 2697 Ma (Lafrance et al., 2005) synvolcanic Mooshla intrusion, west of LaRonde Penna, cuts part of the Hébécourt Formation and the lower part of the Bousquet Formation (Stone 1990; Lafrance et al., 2003a; Galley and Lafrance, 2007).

Several petrogenetic models have been proposed to explain the formation of the Blake River Group, including the Doyon-Bousquet-LaRonde mining camp area. A low degree of partial fusion of lherzolite followed by magmatic differentiation was proposed by Smith (1980). Jensen (1985) proposed that recycling of sagging mafic rocks (eclogites) at the base of the sequence could have been responsible for the generation of calc-alkaline magmas. Mantle diapirism also has been proposed, in which variations in magma composition are attributed to variations in the fusion conditions (e.g., Capdevila et al., 1982) or to local variations in mantle composition (e.g., Goodwin, 1982). Mantle diapirism in a back-arc extensional setting was suggested by Ujike and Goodwin (1987), Laflèche et al. (1992a, b) and Wyman et al. (2002) to explain the tholeiitic to calc-alkaline magmatism of the Blake River Group. Transitional to calc-alkaline magmas in the upper part of the Blake River Group have mostly been attributed to fractionation of mafic magmas, magma mixing, and, in some cases, to crustal contamination. The presence of older crust beneath the Blake River also has been proposed (Baragar, 1968; Gariépy et al., 1982; Gélinas and Ludden, 1984; Gélinas et al., 1984). This was based on the abundance of rhyolite relative to calc-alkaline andesite, the presence of granodioritic xenoliths in calc-alkaline rocks, and some $^{207}Pb/^{204}Pb$ initial ratios compatible with a slightly older crust. Mercier-Langevin et al. (2007a) reported inherited zircons in the footwall felsic flow breccia of the LaRonde Penna 20 North lens and suggested the presence of a ca. 2721 Ma substratum beneath the 2701 to 2698 Ma Bousquet Formation during its formation.

### *LaRonde Penna deposit*

The LaRonde Penna mine stratigraphy comprises the Hébécourt Formation and the lower and upper members of the Bousquet Formation. The volcanic units of the mine sequence are described elsewhere in detail (Mercier-Langevin et al., 2007a), and only a summary of the upper member units is given here. The geometry, geochemistry, and genesis of the main ore lenses (20 North and 20 South) are described and discussed in more detail by Dubé et al. (2007) and Mercier-Langevin et al. (2007a).

The upper member of the Bousquet Formation is composed of five main stratigraphic units in which the Au-rich sulfide lenses of the deposit are intercalated. The base is mainly composed of dacitic to rhyodacitic flow breccia (unit 5.1b), marking the transition from large-scale mafic tholeiitic to transitional volcanism (Hébécourt Formation and lower member of the Bousquet Formation) to small-scale felsic-dominated transitional to calc-alkaline flows and domes. This dacitic to rhyodacitic flow breccia is intercalated with andesitic flows and cut by mafic sills and dikes. The andesite flows are locally overlain by fine-grained hyaloclastite and thin strata of volcanogenic sedimentary rocks and graphitic argillite. The andesite is cut by dacitic to rhyodacitic domes and lobes. A rhyodacite-rhyolite unit (unit 5.2b) covers the dacite-rhyodacite of unit 5.1b and comprises rhyodacitic to rhyolitic flow breccia and rhyolitic domes and/or cryptodomes partially exposed on surface (Mercier-Langevin et al., 2007a). This rhyolitic unit is temporally associated with the beginning of the hydrothermal activity responsible for the formation of the LaRonde Penna 20 North and Bousquet 2-Dumagami ore lenses at around 2698 Ma (Mercier-Langevin et al., 2007a). Fragments of felsic intrusive rocks that may come from an older basement are found in unit 5.2b. This is supported by the presence of inherited zircons in unit 5.2b (Mercier-Langevin et al., 2007a). The rhyodacite-rhyolite (unit 5.2b) is overlain by the upper felsic unit (5.5), composed of rhyolitic flow breccia cut by a coeval feldspar and quartz-phyric rhyolite cryptodome (unit 5.3). A mafic to intermediate basaltic andesite sill and dike complex (unit 5.4) cuts units 5.5 and 5.3. This volcanic sequence was eroded and covered by turbidites at least 5 to 10 m.y. later, as indicated by the age of the youngest detrital zircons from the Cadillac Group at LaRonde (2689 ± 2 Ma: Mercier-Langevin et al., 2007a).

## Lithogeochemistry

The host sequence is variably altered as a result of locally intense hydrothermal activity followed by upper greenschist to lower amphibolite facies metamorphic recrystallization. The average geochemical compositions of host units, listed in Table 1, were obtained from a selection of least altered samples. Samples were selected according to their position in the host sequence relative to the ore lenses and the distribution of alteration zones, their mineralogical composition, the consistency of their trace elements ratios, and a number of alteration indices (LOI, Ishikawa, chlorite-carbonate-pyrite: Ishikawa et al., 1976; Large et al., 2001). The analytical techniques are summarized in Appendix 1.

### *Hébécourt Formation*

A sample of the Hébécourt Formation north of the LaRonde Penna mine plots in the andesite field, close to basalt, in the classification diagram of Winchester and Floyd (1977) shown in Figure 1A, based on $SiO_2$ versus $Zr/(TiO_2*0.0001)$, and in the basaltic andesite field in the classification diagram of Winchester and Floyd (1977) shown in Figure 1B, based on $Zr/(TiO_2*0.0001)$ versus Nb/Y. Lafrance et al. (2003a) showed that the Hébécourt Formation varies from basaltic to andesitic throughout the Doyon-Bousquet-LaRonde mining camp. Volcanic rocks are tholeiitic according to the AFM diagram of Irvine and Baragar (1971) in Figure 1C and the Zr/Ti versus Y/Ti plot of Lentz (1999) shown in Figure 1D, with a low Zr/Y ratio of 2.65 (Table 1). The Hébécourt Formation is characterized by REE abundances of about 20 to 30× chondritic values with a very slightly LREE depleted chondrite-normalized pattern (Fig. 2A) and a $[La/Sm]_N$ ratio of 0.89 (Table 1). A weak negative Eu anomaly, minor depletion in most incompatible elements (Th, Nb and Ta) relative to LREE, and a pronounced negative Ti anomaly are apparent in these rocks (Fig. 2A).

### *Bousquet Formation, lower member*

Rocks from the lower member of the Bousquet Formation are tholeiitic based on their major element compositions (Fig. 1C) and on the low Zr/Y ratio (2.3–3.5) of each unit (Table 1, Fig. 1D). The felsic sills (unit 2.0) are enriched in LREE ($[La/Yb]_N$ = 2.08), have a negative Eu anomaly, a flat HREE pattern, slightly negative Nb and Ta anomalies, a pronounced negative Ti anomaly, and a positive Th anomaly relative to LREE (Fig. 2A). There are pronounced positive Zr and Hf anomalies in this unit. It plots within the ocean ridge field in the tectonic discrimation diagrams of Pearce et al. (1984) and in the intraplate field in the Th/Ta versus Yb diagram of Gorton and Schandl (2000) shown in Figure 3. Units 3.3 (scoriaceous tuff) and 4.4 (heterogeneous unit) show similar chondrite-normalized REE and trace element patterns characterized by a LREE enrichment, flat HREE at about 8 to 10× chondritic values, weak negative Zr and Hf anomalies, and deep negative Nb and Ta anomalies. The scoriaceous tuff (unit 3.3) is, however, slighty depleted in Th relative to LREE, whereas the heterogeneous unit (unit 4.4) is weakly enriched in Th relative to LREE (Fig. 2A). These units plot in the active continental margin field in the Th/Ta versus Yb diagram of Gorton and Schandl (2000; Fig. 3C).

### *Bousquet Formation, upper member*

The upper member of the Bousquet Formation consists of five different units (5.1–5.5), some of which have been further divided into subunits (see Mercier-Langevin et al., 2007a). Overall, these units range in composition from mafic to intermediate (basaltic andesite) to felsic (dacite, rhyodacite and rhyolite) and are tholeiitic to calc-alkaline with a tholeiitic affinity among the mafic to intermediate units and subunits and a calc-alkaline affinity among the felsic units and subunits.

*Dacite-rhyodacite (unit 5.1b):* The dacite-rhyodacite has been divided into four subunits by Mercier-Langevin (2005) based on field relationships and $Zr/TiO_2$ ratio, which is unaffected by hydrothermal alteration even in strongly altered samples of the LaRonde Penna host sequence (Dubé et al., 2007). The Ti-rich dacite (subunit 5.1b-(a)) has a $Zr/TiO_2$ ratio of 109.7, is dacitic (Fig. 1A) and tholeiitic to transitional (Fig. 1C, D). Rocks from this unit are relatively rich in Ti (1.06 wt % $TiO_2$) and Al (17.24 wt % $Al_2O_3$). The andesite-dacite (subunit 5.1b-(b)) has a $Zr/TiO_2$ ratio of 246.8 and is andesitic to dacitic (Fig. 1A, B) and transitional between tholeiitic and calc-alkaline (Fig. 1C, D). In detail, this subunit is characterized by elevated $TiO_2$ (0.97 wt %) and $Al_2O_3$ (17.43 wt %) and a low $Na_2O/K_2O$ ratio (Table 1). Zr and Y are also elevated compared to the other units of the LaRonde host sequence. The andesite-dacite (subunit 5.1b-(b)) has a

TABLE 1. Average Chemical Composition of Least Altered

| | Hébécourt Fm. | | Lower member of the Bousquet Fm. | | | | | | | | | |
|---|---|---|---|---|---|---|---|---|---|---|---|---|
| | Unit 1.0 $n = 1$ | Felsic sills Unit 2.0 $n = 1$ | Scoriaceous tuff Unit 3.3 $n = 3$ | | Heterogeneous Unit Unit 4.4 $n = 11$ | | Dacite-rhyodacite Subunit 5.1b-(d) $n = 14$ | | Andesitic sills Subunit 5.1b-(c) $n = 5$ | | Andesite-dacite Subunit 5.1b-(b) $n = 5$ | |
| | Mean | Mean | Mean | 2$\sigma$ | Mean | 2$\sigma$ | Mean | 2$\sigma$ | Mean | 2$\sigma$ | Mean | 2$\sigma$ |
| $SiO_2$ (%) | 54.7 | 75.9 | 53.5 | 3.5 | 51.3 | 3.8 | 72.0 | 2.4 | 57.4 | 2.9 | 64.0 | 2.1 |
| $TiO_2$ | 0.91 | 0.28 | 1.00 | 0.26 | 0.93 | 0.23 | 0.64 | 0.07 | 1.39 | 0.18 | 0.97 | 0.10 |
| $Al_2O_3$ | 15.3 | 11.3 | 19.3 | 2.6 | 19.4 | 3.1 | 14.6 | 1.3 | 24.0 | 2.2 | 17.4 | 2.2 |
| $Fe_2O_{3(total)}$ | 9.46 | 3.56 | 9.76 | 2.41 | 8.54 | 1.95 | 1.44 | 0.93 | 2.30 | 1.30 | 3.58 | 0.51 |
| MnO | 0.14 | 0.05 | 0.19 | 0.05 | 0.18 | 0.05 | 0.03 | 0.02 | 0.07 | 0.04 | 0.09 | 0.03 |
| MgO | 6.54 | 1.15 | 2.88 | 0.60 | 3.61 | 2.25 | 0.45 | 0.28 | 0.82 | 0.28 | 1.22 | 0.37 |
| CaO | 9.68 | 2.29 | 7.51 | 1.52 | 10.32 | 2.43 | 1.64 | 0.45 | 6.53 | 0.79 | 4.08 | 1.00 |
| $Na_2O$ | 2.00 | 3.40 | 3.78 | 1.42 | 2.64 | 1.04 | 5.84 | 0.64 | 3.93 | 0.54 | 4.09 | 1.70 |
| $K_2O$ | 0.21 | 1.90 | 0.71 | 0.14 | 0.93 | 0.26 | 1.36 | 0.58 | 1.20 | 0.77 | 2.31 | 0.80 |
| $P_2O_5$ | 0.07 | 0.05 | 0.17 | 0.04 | 0.18 | 0.09 | 0.14 | 0.05 | 0.13 | 0.07 | 0.34 | 0.09 |
| LOI | 2.25 | 2.49 | 2.53 | 0.94 | 2.24 | 1.18 | 0.83 | 0.28 | 1.79 | 0.71 | 1.51 | 0.33 |
| Total | 101.4 | 102.4 | 101.4 | 0.4 | 100.1 | 0.9 | 99.1 | 0.5 | 100.1 | 0.8 | 99.9 | 0.5 |
| S | 0.02 | 0.01 | 0.02 | 0.01 | 0.09 | 0.09 | 0.07 | 0.06 | 0.74 | 0.81 | 0.20 | 0.18 |
| $CO_2$ | 0.01 | 1.36 | 0.76 | 0.28 | 1.09 | 1.00 | 0.36 | 0.27 | 0.09 | 0.10 | 0.23 | 0.19 |
| FeO[1] | 8.51 | 3.20 | 8.79 | 2.17 | 7.68 | 1.76 | 1.30 | 0.83 | 2.07 | 1.17 | 3.22 | 0.46 |
| Y (ppm) | 42.8 | 71.2 | 18.9 | 2.6 | 15.0 | 5.5 | 27.1 | 6.4 | 10.2 | 1.8 | 48.5 | 7.4 |
| Zr | 113.4 | 240.0 | 44.3 | 10.3 | 52.0 | 16.1 | 181.1 | 19.3 | 51.7 | 2.0 | 239.3 | 11.4 |
| Ba | 75.0 | 460.0 | 236.0 | 129.7 | 253.4 | 108.9 | 393.7 | 172.4 | 412.8 | 222.3 | 623.2 | 242.4 |
| V | 260.0 | 10.0 | 309.3 | 47.8 | 246.8 | 25.4 | 55.4 | 23.0 | 323.8 | 42.3 | 79.8 | 39.2 |
| Sc | 35.8 | 8.5 | 29.5 | 1.5 | 27.8 | 3.4 | 10.5 | 3.3 | 27.8 | 5.8 | 16.0 | 3.5 |
| Be | 0.60 | 1.50 | 0.63 | 0.66 | 0.60 | 0.23 | 0.94 | 0.26 | 0.35 | 0.14 | 1.60 | 0.70 |
| Cr | 92.0 | 1.0 | 16.3 | 17.2 | 41.5 | 74.1 | 7.7 | 8.8 | 37.8 | 13.4 | 2.4 | 0.5 |
| Co | 49.0 | 2.0 | 43.0 | 31.8 | 25.3 | 6.8 | 8.4 | 3.6 | 32.8 | 8.4 | 13.2 | 5.7 |
| Ni | 81.0 | 2.0 | 32.0 | 36.7 | 27.8 | 28.9 | 5.3 | 3.1 | 71.8 | 26.5 | 4.6 | 0.9 |
| K | 0.17 | | 0.58 | 0.12 | 0.73 | 0.20 | 1.10 | 0.43 | 1.04 | 0.71 | 2.08 | 0.76 |
| Ti[1] | 5430 | 1679 | 5991 | 1553 | 5555 | 1405 | 3817 | 444 | 8344 | 1054 | 5797 | 619 |
| Sr | 94.6 | 62.9 | 317.0 | 198.3 | 266.4 | 60.7 | 180.1 | 59.8 | 325.8 | 55.9 | 293.6 | 62.4 |
| Cd | 2.00 | 0.50 | 1.67 | 2.02 | 1.02 | 0.36 | 0.61 | 0.21 | 0.60 | 0.22 | 0.60 | 0.22 |
| Rb | 4.6 | 29.3 | 14.0 | 4.9 | 25.3 | 13.1 | 42.9 | 17.3 | 17.0 | 1.6 | 67.9 | 27.7 |
| Nb | 5.41 | 13.80 | 2.86 | 0.40 | 2.80 | 0.28 | 9.11 | 1.09 | 3.13 | 0.66 | 13.93 | 2.02 |
| Cs | 0.44 | 1.10 | 1.00 | 0.54 | 3.88 | 3.84 | 1.65 | 0.74 | 3.15 | 1.77 | 2.46 | 1.03 |
| Hf | 3.26 | 5.80 | 1.04 | 0.40 | 1.07 | 0.14 | 4.23 | 0.55 | 1.28 | 0.18 | 6.52 | 1.51 |
| Ta | 0.36 | 0.85 | 0.13 | 0.04 | 0.14 | 0.02 | 0.53 | 0.06 | 0.17 | 0.03 | 0.82 | 0.15 |
| Pb | 1.87 | 0.02 | 1.62 | 1.36 | 3.57 | 2.12 | 11.84 | 19.17 | 5.85 | 7.28 | 10.36 | 8.49 |
| Th | 0.52 | 3.60 | 0.75 | 0.02 | 1.76 | 0.90 | 9.93 | 1.74 | 2.82 | 0.11 | 10.66 | 2.75 |
| U | 0.16 | 0.90 | 0.20 | 0.01 | 0.51 | 0.23 | 2.37 | 0.49 | 0.65 | 0.06 | 2.72 | 0.83 |
| REE[2] | n = 1 | n = 1 | n =2 | | n = 5 | | n = 13 | | n = 2 | | n = 3 | |
| La | 6.0 | 22.4 | 7.7 | 2.7 | 10.2 | 3.1 | 42.6 | 6.0 | 17.9 | 0.1 | 54.5 | 9.9 |
| Ce | 18.6 | 52.8 | 18.3 | 6.2 | 22.1 | 6.9 | 89.5 | 10.6 | 39.0 | 4.1 | 123.9 | 23.8 |
| Pr | 2.6 | 7.2 | 2.2 | 0.7 | 2.8 | 0.8 | 10.5 | 1.4 | 5.1 | 0.6 | 14.5 | 3.1 |
| Nd | 13.3 | 30.0 | 10.0 | 2.2 | 11.2 | 2.9 | 37.6 | 5.2 | 20.1 | 3.1 | 56.6 | 11.6 |
| Sm | 4.2 | 7.4 | 2.2 | 0.1 | 2.5 | 0.7 | 6.9 | 1.0 | 4.1 | 0.3 | 10.7 | 2.2 |
| Eu | 1.2 | 1.4 | 0.9 | b.d. | 0.8 | 0.2 | 1.6 | 0.2 | 1.3 | b.d. | 2.5 | 0.5 |
| Gd | 5.5 | 9.0 | 2.7 | 0.1 | 2.2 | 0.4 | 5.1 | 1.1 | 3.5 | 0.3 | 9.3 | 1.9 |
| Tb | 0.9 | 1.6 | 0.4 | b.d. | 0.3 | 0.1 | 0.8 | 0.1 | 0.5 | b.d. | 1.3 | 0.3 |
| Dy | 6.8 | 11.0 | 3.1 | 0.1 | 2.2 | 0.3 | 4.6 | 0.9 | 2.8 | 0.2 | 8.3 | 1.5 |
| Ho | 1.5 | 2.2 | 0.7 | b.d. | 0.5 | 0.1 | 0.9 | 0.2 | 0.5 | b.d. | 1.7 | 0.3 |
| Er | 4.4 | 7.1 | 2.0 | b.d. | 1.3 | 0.1 | 2.6 | 0.5 | 1.4 | 0.1 | 5.1 | 1.0 |
| Tm | 0.6 | 1.1 | 0.3 | 0.0 | 0.2 | b.d. | 0.4 | 0.1 | 0.2 | b.d. | 0.8 | 0.1 |
| Yb | 4.1 | 7.3 | 1.8 | 0.2 | 1.2 | 0.1 | 2.8 | 0.6 | 1.4 | 0.1 | 5.2 | 0.9 |
| Lu | 0.6 | 1.1 | 0.3 | b.d. | 0.2 | b.d. | 0.4 | 0.1 | 0.2 | b.d. | 0.8 | 0.2 |
| CCPI[3] | 87 | 45 | 72 | | 76 | | 20 | | 36 | | 41 | |
| AI[4] | 37 | 35 | 24 | | 26 | | 20 | | 16 | | 30 | |
| $Na_2O/K_2O$ | 9.5 | 1.8 | 5.3 | | 2.8 | | 4.3 | | 3.3 | | 1.8 | |
| $Zr/TiO_2$ | 125 | 857 | 44 | | 56 | | 284 | | 37 | | 248 | |
| Zr/Y | 2.65 | 3.37 | 2.34 | | 3.47 | | 6.68 | | 5.06 | | 4.93 | |
| Ti/Zr | 48 | 7 | 135 | | 107 | | 21 | | 161 | | 24 | |
| Zr/Ti | 0.02 | 0.14 | 0.01 | | 0.01 | | 0.05 | | 0.01 | | 0.04 | |
| Y/Ti | 0.01 | 0.04 | 0.00 | | 0.00 | | 0.01 | | 0.00 | | 0.01 | |
| Nb/Y | 0.13 | 0.19 | 0.15 | | 0.19 | | 0.34 | | 0.31 | | 0.29 | |

Host Rocks of the LaRonde Penna Au-Rich VMS Deposit

| | | Upper member of the Bousquet Fm. | | | | | | | | | | | |
|---|---|---|---|---|---|---|---|---|---|---|---|---|---|
| Ti-rich dacite Subunit 5.1b-(a) $n = 3$ | | Rhyodacite-rhyolite Unit 5.2b $n = 4$ | | Rhyolite dome or cryptodome Subunit 5.2b-R $n = 6$ | | Unit 5.2b average $n = 10$ | | Feldspar and quartz-phyric rhyolite Unit 5.3 $n = 5$ | | Basaltic andesite Unit 5.4 $n = 8$ | | Upper felsic Unit Unit 5.5 $n = 5$ | |
| Mean | 2$\sigma$ | Mean | 2$\sigma$ | Mean | 2$\sigma$ | Mean | 2$\sigma$ | Mean | 2$\sigma$ | Mean | 2$\sigma$ | Mean | 2$\sigma$ |
| 64.4 | 3.9 | 70.9 | 1.0 | 74.9 | 1.6 | 73.3 | 2.5 | 75.4 | 1.6 | 56.8 | 4.1 | 73.5 | 2.2 |
| 1.06 | 0.07 | 0.67 | 0.03 | 0.36 | 0.10 | 0.48 | 0.17 | 0.21 | 0.02 | 1.11 | 0.12 | 0.38 | 0.10 |
| 17.2 | 1.2 | 14.5 | 0.6 | 13.5 | 0.8 | 13.9 | 0.9 | 13.1 | 1.6 | 20.4 | 1.2 | 12.7 | 0.7 |
| 4.00 | 2.16 | 2.64 | 1.30 | 1.57 | 0.78 | 2.00 | 1.10 | 1.37 | 0.24 | 4.68 | 2.43 | 1.66 | 0.74 |
| 0.07 | 0.06 | 0.07 | 0.04 | 0.05 | 0.02 | 0.06 | 0.03 | 0.03 | b.d. | 0.07 | 0.03 | 0.04 | 0.02 |
| 1.14 | 0.99 | 0.57 | 0.31 | 0.44 | 0.21 | 0.49 | 0.24 | 0.40 | 0.08 | 3.14 | 1.24 | 0.41 | 0.17 |
| 3.75 | 2.70 | 1.94 | 0.32 | 1.46 | 0.44 | 1.65 | 0.45 | 2.61 | 1.33 | 5.10 | 2.17 | 2.34 | 0.71 |
| 2.29 | 1.12 | 5.64 | 1.00 | 4.47 | 1.11 | 4.94 | 1.18 | 3.73 | 1.75 | 5.15 | 1.16 | 3.31 | 1.22 |
| 2.72 | 1.70 | 1.69 | 0.84 | 2.35 | 1.16 | 2.09 | 1.05 | 1.57 | 0.62 | 1.12 | 0.64 | 2.29 | 0.62 |
| 0.31 | 0.06 | 0.16 | 0.02 | 0.07 | 0.02 | 0.10 | 0.05 | 0.04 | 0.01 | 0.12 | 0.02 | 0.06 | 0.02 |
| 2.28 | 0.47 | 0.69 | 0.41 | 1.34 | 0.62 | 1.08 | 0.62 | 1.26 | 0.69 | 1.84 | 0.65 | 1.37 | 0.80 |
| 99.6 | 1.1 | 99.5 | 0.8 | 100.6 | 1.9 | 100.1 | 1.6 | 99.7 | 1.0 | 99.7 | 0.6 | 98.5 | 1.0 |
| 0.41 | 0.29 | 0.09 | 0.13 | 0.05 | 0.03 | 0.07 | 0.08 | 0.13 | 0.14 | 0.80 | 0.70 | 0.26 | 0.29 |
| 0.13 | 0.11 | 0.26 | 0.39 | 0.59 | 0.45 | 0.46 | 0.44 | 0.51 | 0.48 | 0.16 | 0.28 | 0.58 | 0.42 |
| 3.60 | 1.94 | 2.38 | 1.17 | 1.41 | 0.70 | 1.80 | 0.99 | 1.23 | 0.21 | 4.21 | 2.19 | 1.49 | 0.67 |
| 30.1 | 10.6 | 33.3 | 7.5 | 24.0 | 7.3 | 27.7 | 8.5 | 18.1 | 3.8 | 11.7 | 2.8 | 23.5 | 4.2 |
| 116.3 | 7.0 | 184.8 | 20.2 | 192.4 | 21.1 | 189.3 | 20.0 | 127.9 | 12.5 | 51.1 | 19.8 | 184.8 | 29.8 |
| 698.7 | 304.1 | 418.1 | 175.5 | 712.5 | 969.4 | 614.4 | 785.3 | 488.4 | 211.2 | 349.5 | 210.4 | 770.6 | 312.5 |
| 154.7 | 28.0 | 46.0 | 28.8 | 14.8 | 13.8 | 25.2 | 23.9 | 12.2 | 2.2 | 308.4 | 22.2 | 35.6 | 27.8 |
| 22.2 | 4.3 | 12.2 | 2.7 | 4.6 | 2.5 | 7.1 | 4.4 | 2.9 | 0.4 | 33.4 | 3.0 | 5.9 | 3.0 |
| 2.00 | 0.20 | 1.24 | 0.57 | 0.83 | 0.32 | 0.97 | 0.43 | 1.38 | 0.23 | 0.45 | 0.13 | 1.06 | 0.25 |
| 58.0 | 40.4 | 2.7 | 1.2 | 2.0 | 0.6 | 2.2 | 0.8 | 2.3 | 2.7 | 90.9 | 20.7 | 3.2 | 1.3 |
| 22.3 | 9.6 | 6.3 | 2.9 | 1.5 | 0.8 | 3.1 | 2.9 | 2.0 | 0.7 | 45.6 | 10.5 | 6.8 | 3.6 |
| 31.0 | 20.9 | 3.0 | 1.0 | 1.5 | 0.5 | 2.0 | 1.0 | 2.4 | 2.2 | 112.6 | 22.2 | 4.4 | 1.1 |
| 3.36 | | 1.35 | 0.12 | 2.08 | 2.44 | 1.90 | 2.09 | 1.09 | 0.79 | 0.95 | 0.54 | 1.91 | 0.48 |
| 6353 | 412 | 3959 | 243 | 2262 | 524 | 2828 | 952 | 1246 | 106 | 6677 | 718 | 2270 | 623 |
| 292.0 | 137.6 | 190.1 | 105.6 | 113.0 | 27.8 | 138.7 | 69.0 | 270.2 | 55.9 | 259.4 | 56.2 | 192.2 | 104.3 |
| 2.67 | 3.75 | 0.50 | 0.00 | 1.00 | 0.00 | 0.83 | 0.25 | 0.80 | 0.27 | 0.75 | 0.27 | 0.50 | 0.00 |
| | | 50.1 | 11.6 | 32.5 | 21.7 | 25.5 | 15.6 | 71.8 | 21.5 | 40.0 | 38.9 | 76.2 | 17.8 |
| | | 10.09 | 0.98 | 12.07 | 2.91 | 12.11 | 4.04 | 12.37 | 1.88 | 4.20 | 0.89 | 11.80 | 2.59 |
| | | 2.92 | 1.84 | 1.00 | 1.25 | 0.55 | 0.34 | 1.89 | 1.46 | 1.67 | 1.43 | 2.40 | 0.92 |
| | | 4.85 | 0.55 | 4.45 | 0.73 | 4.28 | 0.66 | 3.03 | 0.24 | 1.35 | 0.40 | 4.06 | 0.66 |
| | | 0.61 | 0.08 | 0.77 | 0.21 | 0.76 | 0.29 | 0.94 | 0.18 | 0.24 | 0.07 | 0.74 | 0.20 |
| | | 47.80 | 131.54 | 30.62 | 58.37 | 6.14 | 1.25 | 5.52 | 2.70 | 115.52 | 320.89 | 9.11 | 5.41 |
| | | 8.52 | 1.03 | 11.10 | 1.75 | 11.64 | 2.52 | 11.66 | 0.72 | 2.09 | 1.23 | 11.08 | 2.14 |
| | | 2.05 | 0.24 | 3.13 | 2.64 | 2.71 | 0.49 | 2.62 | 0.37 | 0.57 | 0.28 | 2.60 | 0.48 |
| | | n = 14 | | n = 10 | | n = 24 | | n = 7 | | n = 12 | | n = 9 | |
| | | 38.6 | 3.9 | 41.8 | 9.5 | 46.0 | 8.4 | 39.1 | 14.3 | 11.6 | 4.5 | 43.6 | 8.0 |
| | | 84.0 | 6.5 | 84.0 | 14.1 | 91.4 | 13.1 | 72.1 | 28.4 | 25.6 | 9.8 | 86.3 | 12.2 |
| | | 10.1 | 0.8 | 9.7 | 1.5 | 10.3 | 1.5 | 7.5 | 3.0 | 3.2 | 1.1 | 9.7 | 1.7 |
| | | 38.0 | 2.8 | 33.1 | 4.6 | 35.4 | 4.0 | 23.1 | 9.4 | 12.8 | 3.8 | 33.7 | 7.2 |
| | | 7.6 | 0.7 | 6.0 | 1.0 | 6.4 | 0.7 | 3.7 | 1.3 | 2.8 | 0.6 | 5.9 | 1.5 |
| | | 1.8 | 0.1 | 1.3 | 0.3 | 1.4 | 0.1 | 0.7 | 0.2 | 1.0 | 0.2 | 1.3 | 0.2 |
| | | 6.7 | 1.0 | 4.5 | 0.8 | 4.6 | 0.4 | 2.7 | 1.0 | 2.5 | 0.4 | 4.6 | 1.4 |
| | | 1.0 | 0.2 | 0.7 | 0.1 | 0.7 | 0.1 | 0.4 | 0.1 | 0.4 | 0.1 | 0.7 | 0.2 |
| | | 6.5 | 1.0 | 4.3 | 1.1 | 4.3 | 0.6 | 2.7 | 0.4 | 2.4 | 0.4 | 4.1 | 1.3 |
| | | 1.3 | 0.2 | 0.9 | 0.3 | 0.9 | 0.2 | 0.6 | 0.1 | 0.5 | 0.1 | 0.8 | 0.3 |
| | | 4.0 | 0.7 | 2.6 | 0.9 | 2.5 | 0.5 | 1.8 | 0.2 | 1.3 | 0.3 | 2.5 | 0.8 |
| | | 0.6 | 0.1 | 0.4 | 0.2 | 0.4 | 0.1 | 0.3 | b.d. | 0.2 | b.d. | 0.4 | 0.1 |
| | | 4.3 | 0.8 | 2.9 | 1.1 | 2.7 | 0.6 | 2.1 | 0.2 | 1.3 | 0.3 | 2.7 | 0.8 |
| | | 0.7 | 0.1 | 0.5 | 0.2 | 0.4 | 0.1 | 0.4 | b.d. | 0.2 | 0.1 | 0.4 | 0.1 |
| 49 | | 29 | | 21 | | 25 | | 23 | | 54 | | 25 | |
| 39 | | 23 | | 32 | | 28 | | 24 | | 29 | | 32 | |
| 0.8 | | 3.3 | | 1.9 | | 2.4 | | 2.4 | | 4.6 | | 1.4 | |
| 110 | | 278 | | 535 | | 393 | | 615 | | 46 | | 488 | |
| 3.87 | | 5.55 | | 8.03 | | 6.84 | | 7.05 | | 4.35 | | 7.86 | |
| 55 | | 21 | | 12 | | 15 | | 10 | | 131 | | 12 | |
| 0.02 | | 0.05 | | 0.09 | | 0.07 | | 0.10 | | 0.01 | | 0.08 | |
| 0.00 | | 0.01 | | 0.01 | | 0.01 | | 0.01 | | 0.00 | | 0.01 | |
| | | 0.30 | | 0.50 | | 0.44 | | 0.68 | | 0.36 | | 0.50 | |

TABLE 1.

| | Hébécourt Fm. | | Lower member of the Bousquet Fm. | | | | | | | | | |
|---|---|---|---|---|---|---|---|---|---|---|---|---|
| | Unit 1.0 $n = 1$ | Felsic sills Unit 2.0 $n = 1$ | Scoriaceous tuff Unit 3.3 $n = 3$ | | Heterogeneous Unit Unit 4.4 $n = 11$ | | Dacite-rhyodacite Subunit 5.1b-(d) $n = 14$ | | Andesitic sills Subunit 5.1b-(c) $n = 5$ | | Andesite-dacite Subunit 5.1b-(b) $n = 5$ | |
| | Mean | Mean | Mean | $2\sigma$ | Mean | $2\sigma$ | Mean | $2\sigma$ | Mean | $2\sigma$ | Mean | $2\sigma$ |
| Nb/U | 33.3 | 15.3 | 14.1 | | 5.5 | | 3.8 | | 4.9 | | 5.1 | |
| Nb/Th | 10.4 | 3.8 | 3.8 | | 1.6 | | 0.9 | | 1.1 | | 1.3 | |
| Sc/Yb | 8.7 | 1.2 | 16.4 | | 22.3 | | 3.7 | | 20.0 | | 3.1 | |
| Hf/Sm | 0.78 | 0.78 | 0.46 | | 0.43 | | 0.61 | | 0.31 | | 0.61 | |
| Th/Ta | 1.5 | 4.2 | 5.7 | | 12.9 | | 18.8 | | 16.6 | | 13.0 | |
| Th/La | 0.09 | 0.16 | 0.10 | | 0.17 | | 0.23 | | 0.16 | | 0.20 | |
| [La/Lu]n[5] | 0.96 | 2.08 | 2.82 | | 5.50 | | 9.91 | | 8.63 | | 6.87 | |
| [La/Sm]n[5] | 0.89 | 1.89 | 2.15 | | 2.59 | | 3.86 | | 2.71 | | 3.18 | |
| [La/Yb]n[5] | 0.98 | 2.08 | 2.89 | | 5.55 | | 10.22 | | 8.71 | | 7.14 | |
| [Gd/Lu]n[5] | 1.05 | 0.99 | 1.19 | | 1.40 | | 1.43 | | 2.02 | | 1.40 | |
| Eu/Eu*[6] | 0.76 | 0.52 | 1.06 | | 0.97 | | 0.78 | | 0.99 | | 0.73 | |

[1] Calculated from $Fe_2O_3$, assuming all iron is present as FeO; Ti calculated from $TiO_2$
[2] Number of analyses of REE can differ from those considered in the protolith signature
[3] CCPI = chlorite-carbonate-pyrite index = 100*[(MgO + FeO)/(MgO + FeO + $K_2O$ + $Na_2O$)] (Large et al., 2001)
[4] AI = Hashimoto alteration index = 100*[(MgO + $K_2O$)/(MgO + $K_2O$ + $Na_2O$ + CaO)] (Ishikawa et al., 1976)
[5] Normalized to C1 chondrite value (McDonough and Sun, 1995)
[6] Eu/Eu* = [Eu]N/([Gd]N + [Sm]N)0.5
b.d. = below detection

chondrite-normalized REE pattern characterized by a strong LREE and trace element enrichment ($[La/Yb]_N$ = 7.14; Table 1, Fig. 2B), relatively flat HREE ($[Gd/Lu]_N$ = 1.40) at about 30 to 35× chondritic values, negative Nb and Ta anomalies, positive Zr and Hf anomalies, and weak Eu depletion. Due to high Th (10.66 ppm) and Ta (0.82 ppm) contents, this subunit plots in the active continental margin field of Gorton and Schandl (2000; Fig. 3C). The andesitic sills (subunit 5.1b-(c)) are defined by a clearly distinctive $Zr/TiO_2$ ratio of 37.2 due to a very low concentration in Zr (51.74 ppm). This subunit is basaltic to andesitic (Fig. 1A) and transitional between tholeiitic and calc-alkaline (Fig. 1C, D) with a Zr/Y ratio of 5.06 (Table 1) and elevated $TiO_2$ and $Al_2O_3$. Subunit 5.1b-(c) is characterized by moderately enriched LREE ($[La/Sm]_N$ = 2.71) and fractionated HREE ($[Gd/Lu]_N$ = 2.02), with negative Nb, Ta, Zr, Hf, and Y anomalies and a positive Th anomaly relative to LREE (Fig. 2B). This unit plots within the volcanic-arc field in the tectonic discrimination diagrams of Pearce et al. (1984) and in the intraplate field in the Th/Ta versus Yb diagram of Gorton and Schandl (2000) shown in Figure 3.

The dacite-rhyodacite (subunit 5.1b-(d)) is intercalated with or cut by the three other subunits of unit 5.1b (Mercier-Langevin et al., 2007a). It can be distinguished easily from the other three subunits by its high $SiO_2$ (72 wt %) and low $TiO_2$ concentration (0.64 wt %) and by an elevated $Zr/TiO_2$ ratio (282.9) relative to the other rocks of unit 5.1b. This subunit consists of transitional to calc-alkaline dacite or rhyodacite (Fig. 1C, D), which plots in the volcanic arc fields of tectonic discrimination diagrams of Pearce et al. (1984) or in the active continental margin field of Gorton and Schandl (2000) classification shown in Figure 3. The chondrite-normalized plot is characterized by LREE enrichment ($[La/Yb]_N$ = 10.22), strong negative Nb, Ta, and Ti anomalies (Fig. 2C), weakly negative Eu and Y anomalies, positive Zr and Hf anomalies, a Th enrichment, and relatively flat HREE ($[Gd/Lu]_N$ = 1.43). These features are similar to that of so-called adakites that are found elsewhere in Abitibi (Wyman et al., 2002) but with a slightly lower $Al_2O_3$ concentration and lower $[La/Yb]_N$ ratio.

*Ryodacite-rhyolite (unit 5.2b):* The rhyodacite-rhyolite comprises the immediate footwall of the 20 North lens and hosts the large footwall alteration zone associated with the Au-rich sulfides of this lens (Dubé et al., 2007). Very good surface exposure of a well-preserved section of this unit away from hydrothermal alteration helped define its distribution, mode of emplacement (Mercier-Langevin et al., 2007a), and primary geochemical signature. In particular, a subunit that comprises mainly large domes or cryptodomes within the rhyodacite-rhyolite flow breccia (unit 5.2b) below the 20 North lens (see Mercier-Langevin et al., 2007a) can be distinguished readily on the basis of its $Zr/TiO_2$ ratio. This subunit is characterized by a $Zr/TiO_2$ ratio of 534.4 that is about two times higher than that of the surrounding rhyodacite-rhyolite flow breccia (unit 5.2b, $Zr/TiO_2$ = 275.8; Table 1). Fresh or least

FIG. 1. Major and trace element plots of the average composition of the least altered samples of the host units of the LaRonde Penna mine. A. Discrimination diagram from Winchester and Floyd (1977). B. $Zr/TiO_2$ vs. Nb/Y discrimination diagram from Winchester and Floyd (1977). C. AFM plot (Irvine and Baragar, 1971). D. Zr/Ti vs. Y/Ti plot of tholeiitic vs. calc-alkaline affinity of the felsic volcanic rocks from Lentz (1998).

*(Cont.)*

| | Upper member of the Bousquet Fm. | | | | | | | | | | | | | |
|---|---|---|---|---|---|---|---|---|---|---|---|---|---|---|
| | Ti-rich dacite Subunit 5.1b-(a) $n = 3$ | | Rhyodacite-rhyolite Unit 5.2b $n = 4$ | | Rhyolite dome or cryptodome Subunit 5.2b-R $n = 6$ | | Unit 5.2b average $n = 10$ | | Feldspar and quartz-phyric rhyolite Unit 5.3 $n = 5$ | | Basaltic andesite Unit 5.4 $n = 8$ | | Upper felsic Unit Unit 5.5 $n = 5$ | |
| | Mean | $2\sigma$ | Mean | $2\sigma$ | Mean | $2\sigma$ | Mean | $2\sigma$ | Mean | $2\sigma$ | Mean | $2\sigma$ | Mean | $2\sigma$ |
| | | | 4.9 | | 3.9 | | 4.5 | | 4.7 | | 7.4 | | 4.5 | |
| | | | 1.2 | | 1.1 | | 1.0 | | 1.1 | | 2.0 | | 1.1 | |
| | | | 2.9 | | 1.6 | | 2.7 | | 1.3 | | 26.7 | | 2.2 | |
| | | | 0.64 | | 0.74 | | 0.66 | | 0.82 | | 0.48 | | 0.69 | |
| | | | 14.1 | | 14.5 | | 15.4 | | 12.4 | | 8.9 | | 15.1 | |
| | | | 0.22 | | 0.27 | | 0.25 | | 0.30 | | 0.18 | | 0.25 | |
| | | | 5.97 | | 9.47 | | 11.07 | | 11.55 | | 6.22 | | 10.26 | |
| | | | 3.18 | | 4.34 | | 4.45 | | 6.63 | | 2.55 | | 4.61 | |
| | | | 6.17 | | 9.92 | | 11.66 | | 12.49 | | 6.28 | | 10.96 | |
| | | | 1.22 | | 1.20 | | 1.31 | | 0.96 | | 1.62 | | 1.29 | |
| | | | 0.75 | | 0.72 | | 0.76 | | 0.63 | | 1.09 | | 0.73 | |

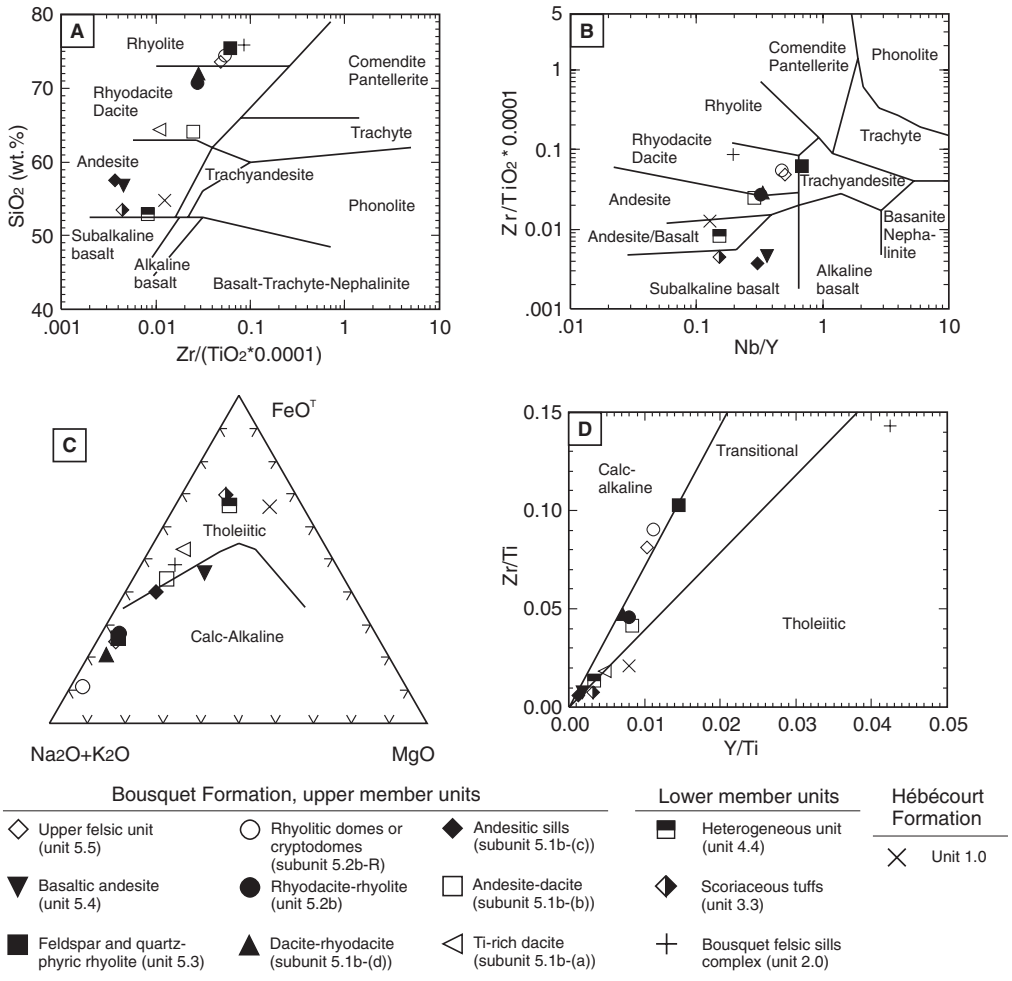

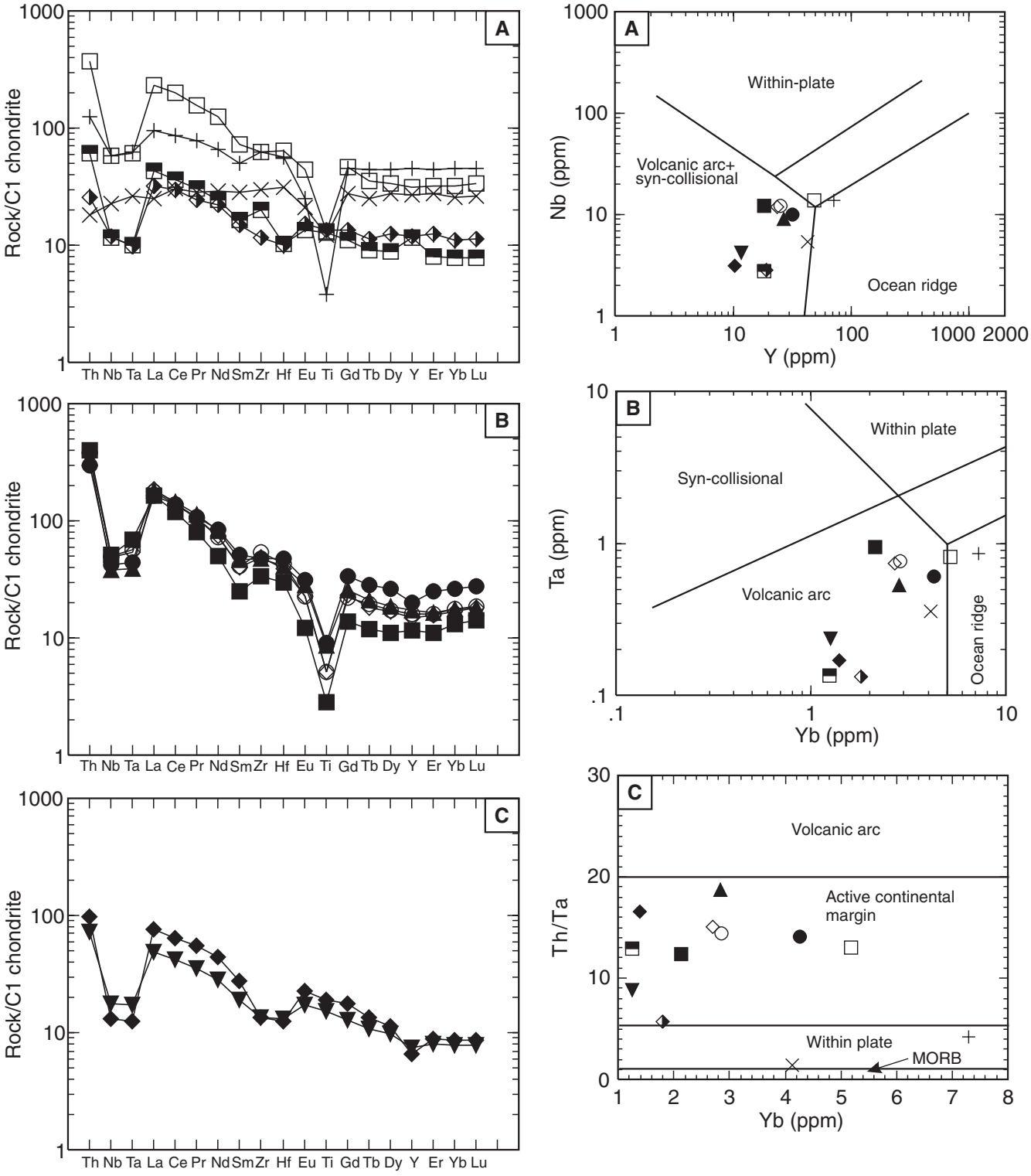


FIG. 2. Chondrite-normalized trace and rare earth element plots for the host units of the LaRonde Penna mine. A. Hébécourt Formation and lower member of the Bousquet Formation. B. Felsic units of the upper member of the Bousquet Formation. C. Mafic to intermediate units of the upper member of the Bousquet Formation. C1 chondrite normalization values from McDonough and Sun (1995). Unit symbols as in Figure 1.

FIG. 3. A. Nb vs. Y tectonic discrimination diagram of Pearce et al. (1984), showing the distribution of the host units of the LaRonde Penna deposit in the volcanic-arc field, except for the Hébécourt Formation and felsic sills (unit 2.0), which plot within or near the ocean ridge field. B. Ta vs. Yb tectonic discrimination diagram of Pearce et al. (1984), showing the distribution of the host units of the LaRonde Penna deposit. C. Th/Ta vs. Yb tectonic discrimination diagram of Gorton and Schandl (2000), showing the distribution of the host volcanic units of the LaRonde Penna deposit in the active continental margin field (see discussion in the text).

altered samples from the domes or cryptodomes (subunit 5.2b-R) are slightly more felsic than the surrounding volcaniclastic rocks of unit 5.2b (Fig. 1A) and have a stronger calc-alkaline affinity (Fig. 1C, D). This suggests that the source magma may have been slightly different (see below).

The chondrite-normalized plots of the rhyodacite-rhyolite (unit 5.2b) and of the rhyolitic domes or cryptodomes (subunit 5.2b-R) show similar trends except for slightly higher HREE in the flow breccia compared to the dome or cryptodome facies (Fig. 2C). Both profiles are characterized by LREE enrichment ($[La/Sm]_N$ = 3.18-4.34), strong negative Nb, Ta, and Ti anomalies (Fig. 2C), weakly negative Eu and Y anomalies, positive Zr and Hf anomalies, a Th enrichment, and flat HREE ($[Gd/Lu]_N$ = 1.20–1.22).

*Feldspar and quartz-phyric rhyolite (unit 5.3):* This unit is a high-silica rhyolite with a $SiO_2$ content of more than 75 wt percent (Table 1, Fig. 1A), reflecting the abundance of blue quartz microphenocrysts (Mercier-Langevin et al., 2007a). This rhyolite has a lower Zr concentration compared to the other felsic units of the upper member of the Bousquet Formation, with less than 130 ppm Zr (Table 1), and is calc-alkaline with a Zr/Y ratio of 7.05 (Fig. 1C, D). The feldspar and quartz-phyric rhyolite is also characterized by low $TiO_2$ and $Al_2O_3$ concentrations of 0.21 and 13.15 wt percent, respectively, suggesting a high degree of magmatic differentiation. The chondrite-normalized REE pattern is characterized by a strong LREE enrichment ($[La/Sm]_N$ = 6.63; Table 1, Fig. 2C), flat HREE ($[Gd/Lu]_N$ = 0.96), strong negative Nb and Ta anomalies, positive Zr and Hf anomalies, weakly negative Eu anomaly, and a strong negative Ti anomaly. As for the rhyodacite-rhyolite (unit 5.2b), the high-silica rhyolite (unit 5.3) plots in the volcanic arc field of Pearce et al. (1984; Fig. 3A, B), and in the active continental margin field of Figure 3C.

*Basaltic andesite (unit 5.4):* The geochemistry of the basaltic andesite contrasts strongly with that of the other units of the upper member of the Bousquet Formation, with low $SiO_2$ and Zr of 56.83 wt. percent and 51.05 ppm, respectively, and elevated $TiO_2$ and $Al_2O_3$ at 1.11 and 20.36 wt. percent, respectively (Table 1). This unit is tholeiitic to calc-alkaline (Fig. 1C), although the trace elements indicate a more tholeiitic affinity (Zr/Y = 4.35; Fig. 1D). The chondrite-normalized pattern of the basaltic andesite (Fig. 2B) is characterized by LREE enrichments ($[La/Yb]_N$ = 6.28), negative Nb, Ta, Zr, Hf, and Y anomalies, and by a slightly positive Eu anomaly. The Th/Ta ratio is slightly lower than that of the other units of the upper member, but it also plots in the active continental margin field of Gorton and Schandl (2000; Fig. 3C).

*Upper felsic unit (unit 5.5):* This unit is rhyolitic (Fig. 1A) and calc-alkaline (Fig. 1C, D) with a Zr/Y ratio of 7.86 (Table 1). It is slightly more felsic than most of the underlying rhyodacite-rhyolite (unit 5.2b) but slightly less felsic than the rhyolite dome or cryptodome facies (subunit 5.2b-R) and coeval feldspar and quartz-phyric rhyolite (unit 5.3), containing 73.55 wt percent $SiO_2$, 0.38 wt percent $TiO_2$, and 184.76 ppm Zr (Table 1). The chondrite-normalized plots of the upper felsic unit have a pattern similar to that of the rhyolitic domes or cryptodomes (subunit 5.2b-R) and are characterized by LREE enrichment ($[La/Sm]_N$ = 4.61), strong negative Nb, Ta, and Ti anomalies (Fig. 2C), weakly negative Eu and Y anomalies, positive Zr and Hf anomalies, Th enrichment, and flat HREE ($[Gd/Lu]_N$ = 1.29).

## Whole-Rock Sm-Nd Isotope Compositions

Six whole-rock samples from the LaRonde Penna deposit host sequence were analyzed for Sm and Nd isotopes. The analytical procedures are described in Appendix 1. These include the heterogeneous unit of the lower member of the Bousquet Formation (unit 4.4), the dacite-rhyodacite (unit 5.1b), the rhyodacite-rhyolite (unit 5.2b), the feldspar and quartz-phyric rhyolite (unit 5.3), the basaltic andesite (unit 5.4), and the upper felsic unit (unit 5.5) of the upper member of the Bousquet Formation. The samples are described in Table 2.

The isotopic values given in Table 3 were calculated for a time (t) of 2700 Ma. The data are plotted in Figure 4 in a $^{147}Sm/^{144}Nd$ versus $^{143}Nd/^{144}Nd$ diagram. The samples define a regression age of 2692 ± 130 Ma ($2\sigma$ errors) with an initial $^{143}Nd/^{144}Nd$ ratio of 0.509299 ± 0.000091 and a mean squared weighted deviation (MSWD) value of 0.25, calculated using Isoplot version 2.49 and the Yorkfit 1 model (York, 1969; Ludwig, 2001). These results suggest that the samples were not affected by any significant hydrothermal alteration.

TABLE 2. Whole-Rock Sm and Nd Isotope Sample Locations and Descriptions

| Sample no. | Unit or subunit | Sample location | Description |
|---|---|---|---|
| LAPL-019-2001 | 4.4 | Level 194 (1940 m below surface) 7182 mE, 3097 mN mine grid | Fp-glomeroporphyritic basalt, weak biotite-hornblende and epidote alteration |
| LAPL-074-2000 | 5.1b-(d) | 688525 mE, 5344378 mN, UTM NAD83 | Fp-phyric dacite-rhyodacite, very weak sercite alteration |
| LAPL-031-2000 | 5.2b-R | 688039 mE, 5344256 mN, UTM NAD83 | Fp-phyric rhyodacite-rhyolite (dome), weak sericite alteration |
| LAPL-126-2000 | 5.3 | Level 86 (860 m below surface) 7478 mE, 2985 mN mine grid | Fp- and Qz-phyric rhyolitic breccia, slightly sericitized with traces of biotite and tourmaline |
| LAPL-212-2001 | 5.4 | 688643 mE, 5344194 mN, UTM NAD83 | Fp-glomeroporphyritic basaltic andesite, weak sericite and chlorite alteration with traces of pyrrhotite |
| LAPL-060-2001 | 5.5 | ddh 3170-04, from 441.3m to 441.5m (7646 mE, 2880 mN mine grid) | Fp-phyric rhyodacitic to rhyolitic breccia, weakly to moderately sericitized with traces of biotite, chlorite and pyrite |

Fp = Feldspar

TABLE 3. Sm and Nd Isotope Data

| Sample no. | Unit or subunit | Nd (ppm) | Sm (ppm) | $^{147}Sm/^{144}Nd_{(0)}$ | $^{143}Nd/^{144}Nd_{(0)}$ | $^{143}Nd/^{144}Nd_{(t)}$ | $\varepsilon_{Nd}$ (t) |
|---|---|---|---|---|---|---|---|
| LAPL-019-2001 | 4.4 | 12.14 | 2.25 | 0.112 | 0.511286 | 0.5092907 | 3.08 |
| LAPL-074-2000 | 5.1b-(d) | 41.13 | 7.59 | 0.1116 | 0.511281 | 0.5092929 | 3.12 |
| LAPL-031-2000 | 5.2b-R | 34.60 | 5.38 | 0.0939 | 0.510961 | 0.5092882 | 3.03 |
| LAPL-126-2000 | 5.3 | 23.33 | 3.44 | 0.0892 | 0.510881 | 0.5092919 | 3.11 |
| LAPL-212-2001 | 5.4 | 17.69 | 3.48 | 0.12 | 0.511432 | 0.5092942 | 3.15 |
| LAPL-060-2001 | 5.5 | 22.77 | 3.56 | 0.0945 | 0.510988 | 0.5093045 | 3.35 |

Notes: t = 2700 Ma, 0 = present day; present-day $^{143}Nd/^{144}Nd$ and $^{147}Sm/^{144}Nd$ reference values of 0.512638 and 0.1967, respectively, for a chondritic reservoir (CHUR) have been used to calculate $\varepsilon_{Nd}(t)$; estimated uncertainty in $\varepsilon_{Nd}(t)$ is approximately ±0.8 epsilon units

*Heterogeneous unit, sample LAPL-019-2001 (unit 4.4):* This sample is from the stratigraphic footwall of the 20 North lens. It is characterized by low Nd and Sm concentrations (12.14 and 2.25 ppm, respectively; Table 3) consistent with the values reported for the least altered samples of unit 4.4 (Table 1), giving an $\varepsilon_{Nd}$ value of 3.08 (Table 3).

*Dacite-rhyodacite, sample LAPL-074-2000 (unit 5.1b):* This sample was collected on surface northeast of the LaRonde Penna mine. Nd and Sm concentrations in this sample are 41.13 and 7.59 ppm, respectively (Table 3), which is consistent with the values reported for the dacite-rhyodacite (subunit 5.1b-(d); Table 1). The isotopic data give an $\varepsilon_{Nd}$ value of 3.12 (Table 3).

*Rhyodacite-rhyolite, sample LAPL-031-2000 (unit 5.2b):* This sample is from the stratigraphic footwall of the 20 North lens on surface, south of the LaRonde Penna mine. Nd and Sm concentrations for this sample are slightly lower than for the dacite-rhyodacite of unit 5.1b at 34.6 and 5.38 ppm, respectively (Table 3). These concentrations are consistent with other samples from the rhyolite dome or cryptodome facies (Table 1). The $\varepsilon_{Nd}$ value is 3.03 (Table 3).

*Feldspar and quartz-phyric rhyolite, sample LAPL-126-2000 (unit 5.3):* This sample is from the stratigraphic hanging wall of the 20 North lens on level 86 (860 m below surface). The analyzed sample contains 23.33 ppm Nd and 3.44 ppm Sm (Table 3) and has an $\varepsilon_{Nd}$ value of 3.11 (Table 3).

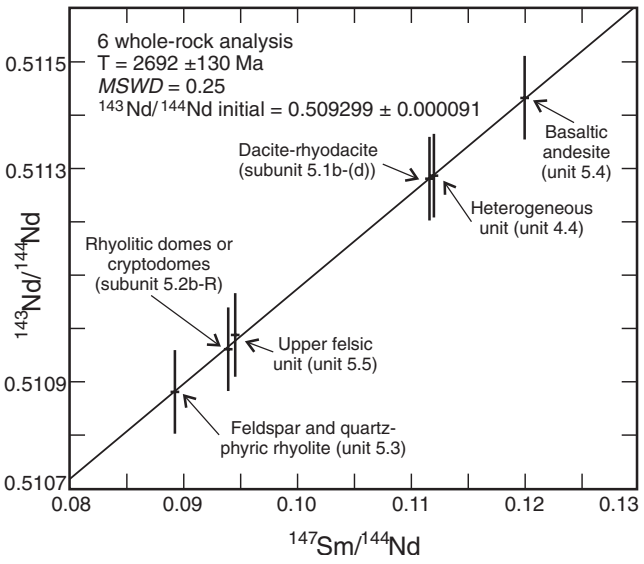


FIG. 4. Whole-rock $^{143}Nd/^{144}Nd$ vs. $^{147}Sm/^{144}Nd$ diagram for selected units of the host volcanic sequence of the LaRonde Penna deposit. Size of cross represents analytical error ($2\sigma$). All samples are within error of the regression line (MSWD = 0.25).

*Basaltic andesite, sample LAPL-212-2001 (unit 5.4):* This sample is from the hanging wall of the 20 North lens and was collected on surface, southeast of the LaRonde Penna mine. It has a relatively low Nd content (17.69 ppm), consistent with its mafic to intermediate composition, but the Sm concentration is relatively high at 3.48 ppm (Table 3). These concentrations are slightly higher than in the other samples of unit 5.4 (Table 1), most likely reflecting the abundance of feldspar phenocrysts in the analyzed sample. The $\varepsilon_{Nd}$ value for this unit is 3.15 (Table 3).

*Upper felsic unit, sample LAPL-060-2001 (unit 5.5):* The Nd and Sm concentrations of this sample are lower than expected for unit 5.5, with 22.77 ppm Nd and 3.56 ppm Sm (Table 3). However, these concentrations are similar to those of the coeval felspar and quartz-phyric rhyolite (unit 5.3). The $\varepsilon_{Nd}$ value of 3.35 is slightly higher than that of unit 5.3 (Table 3).

### *Summary*

All six units have the same $\varepsilon_{Nd}$ values (3.03–3.35), well within the analytical error (± 0.8), suggesting that the sampled units evolved from a common magmatic source derived from a depleted upper mantle at 2.7 Ga (cf. DePaolo, 1981; Goldstein et al., 1984; Nelson and DePaolo, 1984; Stern et al., 1994). This signature is also similar to that of different rocks of the southern Superior province older than 2695 Ma that were derived from a primitive mantle source (cf. Prior et al., 1999b, and references therein). These data suggest that the host rocks of the LaRonde Penna deposit were derived from magmas generated from depleted upper mantle and/or from partial melting of juvenile material (mafic crust) or by a combination of those two sources.

## Petrogenesis of the LaRonde Penna Deposit Host Sequence

### *Hébécourt Formation*

The volcanic rocks of the Hébécourt Formation are slightly more evolved than typical Archean oceanic basalts; their elevated $Al_2O_3$ content is comparable to that of some modern back-arc basin basalts (BABB) and rift-related tholeiites or island-arc basalts (Hochstaeder et al., 1990) and to that of E-MORB (Wilson, 1989). However, the trace elements and REE concentrations are slightly higher than MORB and lower than modern-arc tholeiites, and therefore

are most consistent with slightly depleted back-arc basin basalts. The generation of mafic to intermediate magmas by adiabatic decompression under a relatively thick Archean oceanic lithosphere could produce a weak $Al_2O_3$ enrichment relative to MORB due to the suppression of plagioclase growth at elevated pressure. The similarity of the $[La/Yb]_N$ and Sc/Yb ratios (Fig. 5A, B) to primitive mantle suggests fractional crystallization of clinopyroxene and olivine. The Zr/Y and Th/La ratios (Fig. 5C, D) are also close to those of primitive mantle.

*Bousquet Formation*

The volcanic units of the lower member of the Bousquet Formation are slightly more evolved than the basalt and andesite of the Hébécourt Formation. The tholeiitic felsic rocks of the sill complex (unit 2.0), which intrudes the Hébécourt Formation, could have been generated by low-pressure, high-temperature, low- to moderate-degree partial melting of a tholeiitic mafic source with no residual amphibole (Hart et al., 2004) or garnet (Barrie et al., 1993) followed by plagioclase-dominated fractional crystallization in a subvolcanic magma chamber (Lesher et al., 1986). The tholeiitic felsic sills of unit 2.0 have $[La/Yb]_N$, Zr/Y and Hf/Sm ratios similar to those of mafic rocks of the Hébécourt Formation (Fig. 5), suggesting a common source. Fractional crystallization of plagioclase and Fe-Ti oxides could have led to the formation of tholeiitic, high-silica felsic rocks that can be compared to FIIIa-type rhyolites of Lesher et al. (1986) and of Hart et al. (2004). Weak negative Nb and Ta anomalies, positive Zr and Hf anomalies, and a relative enrichment in Th (Fig. 5F) and LREE (Fig. 2A) may indicate contamination by hydrous magmas and/or assimilation of Nb- and Ta-depleted rocks.

The scoriaceous tuff and the heterogeneous unit of the lower member of the Bousquet Formation (units 3.3 and 4.4) are less differentiated than the underlying units (Fig. 2A). The relative enrichment in LREE and depletion in HREE compared to the tholeiitic to transitional units of the Hébécourt Formation suggest that these predominantly andesitic rocks were not generated by simple fractional crystallization from the same tholeiitic magma reservoir inferred for the Hébécourt Formation and the tholeiitic felsic sills of unit 2.0. This is supported by significant variations of incompatible trace element ratios, such as Sc/Yb, Zr/Y, and Nb/Th (Fig. 5), requiring either a heterogeneous source or contamination (e.g., mixing with mafic to intermediate calc-alkaline magma or slab melts with different trace element ratios) and subsequent fractional crystallization, as suggested by Laflèche et al. (1992b) and by Wyman et al. (2002) for similar rocks of the southern Abitibi belt. The influence of subduction-related processes or crustal contamination is suggested by the Nb/Th and Hf/Sm ratios (Fig. 5G, H) and also by the negative Nb and Ta anomalies (Fig. 2A). The Nb and Ta anomalies alone could be produced during differentiation of tholeiitic rocks after fractional crystallization coupled with contamination-assimilation of a Nb- and Ta-depleted component such as mafic calc-alkaline magmas (Laflèche et al., 1992b). However, similar rocks from the eastern segment of the southern Abitibi belt have been interpreted to be products of the transition from mantle diapirism to subduction-related volcanism by Scott et al. (2002).

The upper member of the Bousquet Formation is characterized by a gradual shift from predominantly mafic tholeiitic transitional volcanism to transitional calc-alkaline felsic-dominated volcanism from the base to the top of the Bousquet Formation (Fig. 5). The mafic rocks include the andesitic sills (subunit 5.1b-(c)) and the basaltic andesite (unit 5.4). The felsic rocks include the dacite-rhyodacite (subunit 5.1b-(d)), the rhyodacite-rhyolite (unit 5.2b), the rhyolitic domes or cryptodomes (subunit 5.2b-R), the feldspar and quartz-phyric rhyolite (unit 5.3), and the upper felsic unit (unit 5.5). Units 3.3 and 4.4 of the lower member of the Bousquet Formation have been grouped with mafic units of the upper member in Figure 5 for comparison.

Rocks from these two groups are characterized by similar chondrite-normalized trace element and REE patterns (Fig. 2B, C) that show LREE enrichments, flat HREE patterns, and negative Nb, Ta, and Ti anomalies. Flat HREE patterns suggest the assimilation of amphibole with chondrite-normalized Gd/Lu ratios close to 1 (Fig. 5I). The felsic units are characterized by positive Zr and Hf anomalies (Fig. 2B), whereas the mafic rocks are characterized by negative Zr and Hf anomalies (Fig. 5) that could indicate the effects of hydrous fluids (metasomatism) in the source from a subducted slab (Wyman et al., 2002). These REE signatures (Fig. 2) are generally attributed to subduction processes and are typical of oceanic arc–back-arc volcanism. However, the Th content of these rocks is higher than would be expected for oceanic arc rocks (Fig. 5D), which explains the misclassification as active continental margin arcs in some diagrams (e.g., Gorton and Schandl, 2000; Fig. 3C). The Th/La ratios of the mafic rocks (Th/La = 0.16–0.19; Table 1, Fig. 5D) suggest a minor assimilation-contamination component or dehydration and partial melting of a metabasaltic source (hydrous metasomatism). This is more important for the felsic rocks (Th/La = 0.22–0.30; Fig. 5D). Assimilation-contamination is also suggested by the low Nb/Th and Nb/U ratios relative to primitive mantle and MORB (Fig. 5F, G).

The LaRonde Penna host felsic rocks have a number of geochemical similarities to modern ensialic arcs (Fig. 6A) in which the subduction-related magmas are contaminated by continental crust. Similar felsic rocks host the Early Proterozoic Boliden Au-As deposit of the Skellefte district in Sweden (Weihed et al., 1992; Allen et al., 1996; Bergman Weihed et al., 1996; Billstrom and Weihed, 1996). Crustal contamination by continental material at LaRonde Penna is not likely, as the $\varepsilon_{Nd}$ values for the felsic rocks indicate a depleted asthenospheric or upper mantle source. However, contributions from older or primitive arc–back-arc crust would not have shifted the $\varepsilon_{Nd}$ values significantly (e.g., Barrie et al., 1999). Assimilation of such older crust is suggested by the 2721 Ma inherited zircons in the rhyodacite-rhyolite (unit 5.2b; Mercier-Langevin et al., 2007a) from the footwall of the 20 North lens and by some accidental, subrounded to rounded clasts of felsic intrusive rocks found in flow breccia of unit 5.2b (Mercier-Langevin et al., 2007a: Fig. 5F).

## Geodynamic Setting

The petrogenetic evolution of the volcanic units of the LaRonde Penna mine area, the U-Pb age determinations, the Sm-Nd isotope data, and the inferred geodynamic context

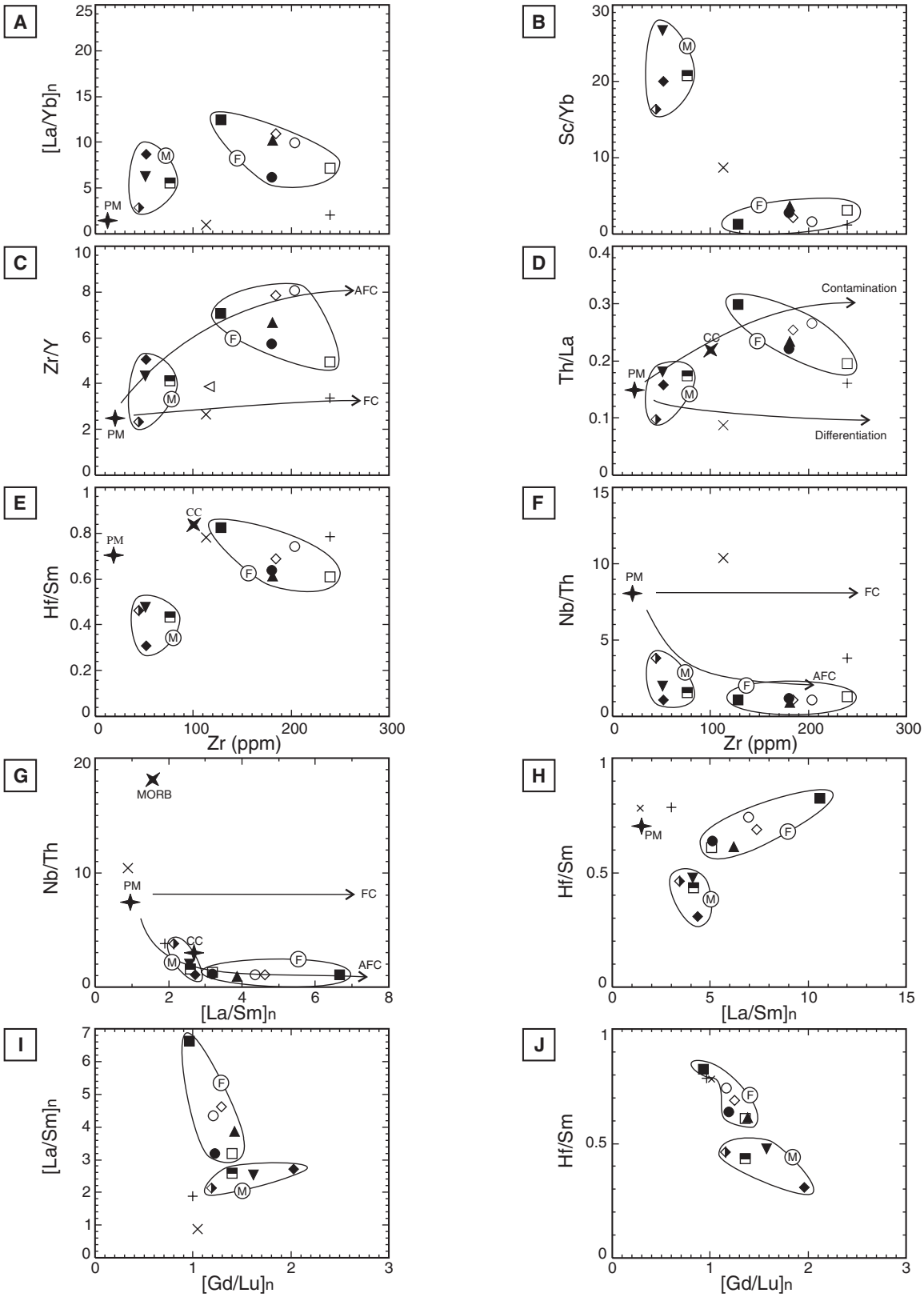


FIG. 5. Ratios of moderately to highly incompatible trace elements plotted against Zr and against REE ratios. These ratios illustrate the magmatic differentiation between the mafic to intermediate and felsic volcanic rocks and between each unit of host rocks of the LaRonde Penna deposit and the processes that may be involved in this differentiation. AFC = assimilation and fractional crystallization, CC = average continental crust, FC = fractional crystallization, F = felsic rocks group, M = mafic rocks group, PM = primitive mantle. Unit symbols as in Figure 1.

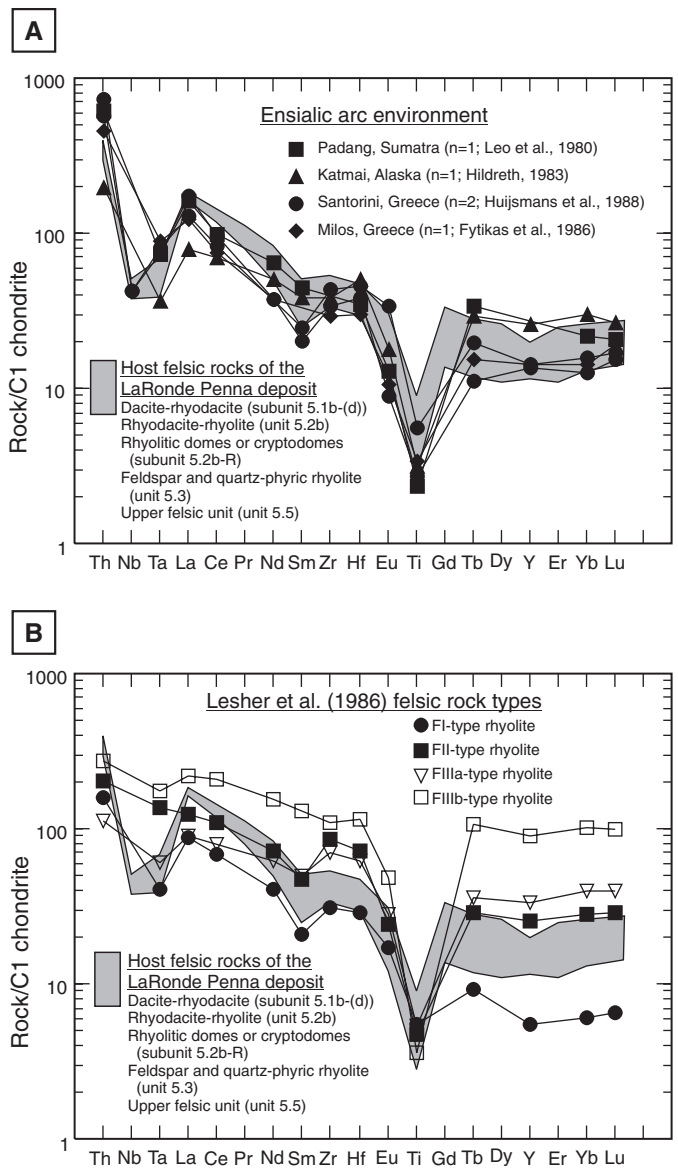


FIG. 6. A. Chondrite-normalized REE-high field strength element diagram of representative ensialic arc samples (after Prior et al., 1999a) plotted against the pattern defined by the felsic rocks of the upper member of the Bousquet Formation, showing the geochemical similarities between the felsic rocks at LaRonde and those formed in ensialic arc environments. B. Chondrite-normalized REE-high field strength element diagram of FI-, FII-, and FIIIa-b-type rhyolites of Lesher et al. (1986) plotted against the pattern defined by the felsic rocks host of the LaRonde Penna mine. This diagram shows the geochemical similarities between the FII rhyolites and the LaRonde felsic volcanic rocks. C1 chondrite normalization values from McDonough and Sun (1995). Unit symbols as in Figure 1.

of the Abitibi greenstone belt help constrain the possible magmatic and tectonic setting of the host sequence of the Doyon-Bousquet-LaRonde mining camp within the Blake River Group of the Abitibi subprovince. The 2701 to 2696 Ma Blake River Group volcanic rocks were emplaced during a late stage of rifting and an early stage of subduction in a back-arc setting following a period of tholeiitic mafic and komatiitic plume-related oceanic plateau volcanism and intra-oceanic arc volcanism between 2730 and 2705 Ma (Laflèche et al., 1992a, b; Ayer et al., 2002; Mueller and Mortensen, 2002; Wyman et al., 2002). Stratigraphic and geochronological relationships suggest that the 2699 to 2698 Ma Bousquet Formation represents the upper part of the Blake River Group (Lafrance et al., 2003a; 2005; Mercier-Langevin et al., 2007a).

The subaqueous tholeiitic basaltic to andesitic rocks of the Hébécourt Formation may have been generated by magma underplating following mantle diapirism related to extension during the last episode of oceanic plateau volcanism, as proposed by Dimroth et al. (1982, 1983a, b) and Wyman (1999). Subduction-related processes or assimilation of Nb- and Ta-depleted material is suggested by the appearance of negative Nb and Ta anomalies in felsic intrusive rocks (e.g., unit 2.0 tholeiitic felsic sills). Fractional crystallization and assimilation-contamination of mafic tholeiitic magma in the crust at low pressure could have formed the felsic sills of unit 2.0. Underplating of a thickened arc crust would have caused partial melting of the crust and the formation of hybrid magmas. Low-degree partial melting of mafic juvenile material, partial melting of mafic to intermediate calc-alkaline rocks, or partial melting of felsic rocks coupled with partial melting of depleted upper mantle wedge and fractional crystallization of amphibole ± plagioclase at midcrustal levels could have produced tholeiitic to transitional, mafic to intermediate rocks of units 3.3 (scoriaceous tuff) and 4.4 (heterogeneous unit) that clearly differ from the underlying rocks. These units were emplaced as extensive subaqueous autoclastic to possibly pyroclastic flows (Stone, 1990) from coalesced effusive centers (Lafrance et al., 2003a). The negative Nb and Ta anomalies that characterize the scoriaceous tuff (unit 3.3) and the heterogeneous unit (unit 4.4) could be related to partial melting of a subducted slab or to the assimilation of some Nb- and Ta-depleted material from the crust. However, the assimilated crust must have been primitive, as the $\varepsilon_{Nd}$ value of unit 4.4 (heterogeneous unit) is that of primitive mantle. The generation of these rocks at midcrustal levels (e.g., 10–15 km) suggests the development of a thickened arc crust and a subsidiary magma chamber. Subsequent fractional crystallization and assimilation in this chamber is believed to have been responsible for the generation of the transitional to calc-alkaline felsic rocks of the Bousquet Formation. A late reintroduction of tholeiitic magma in the emptying subsidiary magma chamber could explain the emplacement of the transitional mafic units (mainly dikes and shallow sills) of the upper member of the Bousquet Formation, which are compositionally similar to the scoriaceous tuff (unit 3.3) of the lower member of the Bousquet Formation. This evolution is compatible with that of a back-arc basin setting where volcanism is first induced by crustal extension and mantle diapirism under a thickened arc crust and later by subduction processes and differentiation in midcrustal magma chambers. This differs slightly from the magmatic evolution in the Noranda area, west of the Doyon-Bousquet-LaRonde mining camp, where the felsic rocks are considered to be the products of low-pressure melting of tholeiitic basalts (Hart et al., 2004) under a thin, immature island-arc crust (Yang and Scott, 2003). However, it can be compared to the evolution of the 2714 to 2702 Ma eastern segment of the Abitibi greenstone belt, as proposed by Scott et al. (2002), who suggested a gradual shift from plume-related volcanism to arc rifting for the Val-d'Or area about 50

km east of the Doyon-Bousquet-LaRonde mining camp. Figure 7 summarizes the possible geodynamic setting of the LaRonde Penna mine host sequence relative to the inferred magmatic and tectonic setting of the Noranda area after Yang and Scott (2003).

### Possible Relationships between Magmatism, Volcanism, and Au-Rich VMS Deposits of the Doyon-Bousquet-LaRonde Mining Camp

In general, VMS deposits hosted by felsic volcanic rocks are thought to have formed in extensional environments of island arcs and continental margins (Hannington et al., 2005), each setting being characterized by volcanic rocks having distinct geochemical signatures (Franklin et al., 2005, and references therein). VMS deposits associated with felsic rocks are genetically linked to the felsic magmatism of particular tectonic settings, and this may explain the provinciality of certain Au-rich VMS deposits, such as in the Doyon-Bousquet-LaRonde camp with four major (>1 Moz Au) Au-rich VMS deposits (Bousquet, Bousquet 2, Dumagami, and LaRonde Penna).

Parallel studies of the ore zones at LaRonde Penna and Bousquet 2 have shown that Au was introduced as part of the volcanogenic hydrothermal mineralizing system and precipitated along with the other metals in response to the chemical and physical conditions of the local geologic setting (Dubé et al., 2007; Mercier-Langevin et al., 2007a). Other Archean VMS deposits are preferentially associated with felsic volcanic rocks characterized by low Zr/Y and $[La/Yb]_N$ ratios, elevated HREE content, and silica-rich compositions, indicative of a high-temperature and relatively low-pressure melting (e.g., Lesher et al., 1986; Barrie et al., 1993; Barrett and MacLean, 1994; Hart et al., 2004). In contrast, the Au-rich VMS deposits of the Doyon-Bousquet-LaRonde mining camp are related to HREE-depleted and high Th felsic rocks that may have been generated by partial melting at high pressure of mafic to intermediate material (garnet in the source) and subsequent fractional crystallization or by partial melting at midcrustal levels (e.g., 10–15 km) caused by ascending mafic to ultramafic magma, following the models of Lesher et al. (1986) and Hart et al. (2004) for the generation of FII-type rhyolites. Yang and Scott (2003) speculated about the possibility that felsic magmas, by degassing metal-rich magmatic fluids, contribute metals to the formation of VMS deposits, and categorized the felsic host rocks of VMS into low, intermediate, and high Th rhyolites (see Table 4). In this classification, the low Th rhyolites, which are common in the Abitibi and especially in the Noranda camp, are characterized by low concentrations of incompatible elements ($[La/Yb]_N$ <3), low Th/Th* ratios (<3), and are associated with Cu ± Zn deposits (Table 4). The intermediate Th rhyolites, which are common in the Hokuroku district of Japan and in the central Abitibi subprovince, are characterized by moderate Th/Th* (3–8) and ($[La/Yb]_N$ = 2–6) and by an association with Cu + Zn ± Pb deposits, whereas the high Th rhyolites are typical of the sediment-influenced Iberian Pyrite Belt and Bathurst camp. The latter are characterized by high concentrations of incompatible

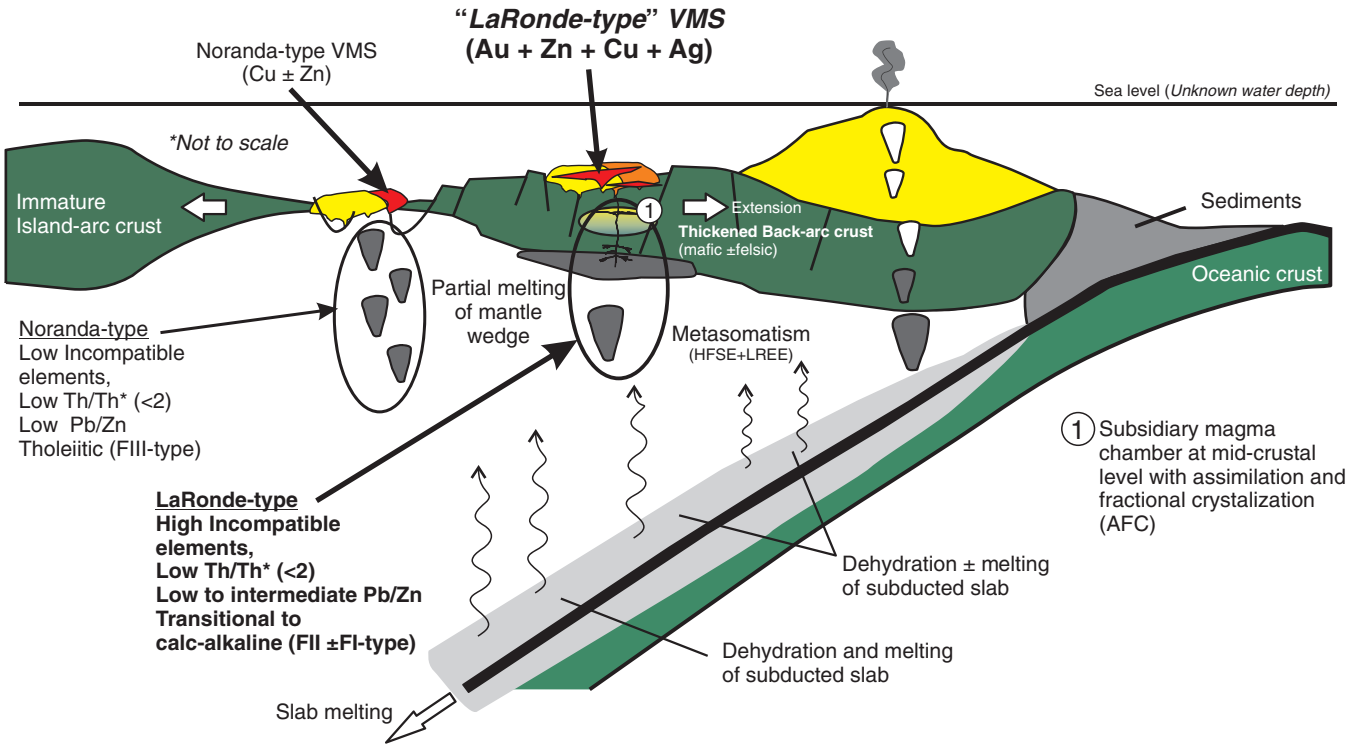


FIG. 7. Schematic geodynamic and tectonic setting for the LaRonde Penna deposit and Doyon-Bousquet-LaRonde mining camp Au-rich VMS deposits compared to the inferred magmatic and tectonic setting for Noranda-type VMS deposits. The geodynamic model proposed for the LaRonde-type VMS involves the development of a subsidiary magma chamber at midcrustal level with assimilation and subsequent fractional crystallization in a thickened crust in extension. Modified from Yang and Scott (2003).

TABLE 4. Comparison of the LaRonde-Type VMS Deposit with that of the Main Types of VMS Deposits Associated with Felsic Rocks of Bimodal Suites Defined by Yang and Scott (2003)

| | Noranda-type VMS deposit | Kuroko-type VMS deposit | Bathurst-type VMS deposit | LaRonde-type VMS deposit |
|---|---|---|---|---|
| Host sequence | Dominantly mafic (>85%) | Variably felsic (15–85%) | Dominantly felsic (>65%) | Variably felsic (±50 %) |
| Classification [1] | Bimodal mafic | Bimodal felsic | Siliciclastic felsic | Bimodal felsic |
| $\varepsilon_{Nd}$ [2,3,4] | 2 to 3.1 | 2 to 8.3 | –5.8 to –2.6 | 3 to 3.4 |
| Felsic rocks | | | | |
| Affinity | Calc-alkaline or transitional dacite and rhyolite | Calc-alkaline dacite and rhyolite | Calc-alkaline dacite and rhyolite | Transitional to calc-alkaline dacite, rhyodacite and rhyolite |
| Type [5] | FIIIa and FIIIb | FII | FII | FII (±FI) |
| Type [6] | Group I | Group II-III | Group IV | Group III |
| $Na_2O/K_2O$ | <2 (low $K_2O$) | Variable (avg. <1) | Mostly <1 (high $K_2O$) | Moderate (1.5–4.5) |
| Th trend | Low Th | Intermediate Th | High Th | High Th |
| [La/Yb]n ratio [7] | <3 | 2 to 6 | >4 | 6 to 13 |
| Th/Th* ratio [8] | <3 | 3 to 8 | >8 | <2 |
| Mafic rocks | Tholeiitic basalt | Tholeiitic to transitional (high Al basalt) | Continental tholeiitic, alkalic basalt | Tholeiitic to transitional |
| Composition of deposits | | | | |
| Base metals | Cu ± Zn | Cu + Zn ± Pb | Pb + Zn + Cu (Sn) | Zn + Cu ± Pb |
| Pb/Zn | Low (<0.1) | Intermediate (<0.1–0.3) | High (0.3–0.5) | Low (<0.12) |
| Au and Ag | High | Variable | Low | Very high |
| Inferred tectonic setting | Back-arc basin on an immature mafic island arc crust | Back-arc basin in a mature felsic-mafic island arc crust | Back-arc basin in felsic continental crust | Back-arc basin in a thick mafic (±felsic) island arc crust |

[1] Franklin et al. (2005)
[2] Vervoot et al. (1994)
[3] Nohda and Wasserburg (1981)
[4] Rogers et al. (2003)
[5] Lesher et al. (1986)
[6] Barrie et al. (1993)
[7] Normalized to chondrite C1 (McDonough and Sun, 1995)
[8] $Th/Th^* = (Th)_N/(Zr_N + Hf_N)^{0.5}$ (Yang and Scott, 2003)

elements ($[La/Yb]_N$ >4), high Th/Th* ratios (>8), and are associated with Pb + Zn + Cu deposits. The high Th and incompatible element content ($[La/Yb]_N$ = 6–13) of the host rocks at LaRonde Penna are more typical of VMS deposits in sediment-influenced continental margin arc or mature arc–back-arc environments than the Noranda-type (immature arc–back-arc) extensional environment (Table 4). The metal content of the deposits could be related to the difference between the inferred geodynamic setting of the Doyon-Bousquet-LaRonde (Table 4) and the Noranda-type setting. As shown in Figure 7, and based on the petrogenetic evolution of the host rocks, it is proposed that the Doyon-Bousquet-LaRonde volcanic sequence was formed in a setting intermediate between back-arc basin and volcanic arc environments. We speculate that this particular position, closer to the subduction zone in an arc–back-arc system, may be responsible, at least in part, for the Au enrichment of the VMS deposits of the Doyon-Bousquet-LaRonde mining camp. A position closer to an arc may imply shallower water depth, which could induce boiling, but also a possible affinity with arc-related, calc-alkaline and volatile-rich Au-bearing magmas such as in porphyry and epithermal systems for which a direct magmatic contribution to the ore fluids is recognized (e.g., Sillitoe, 1993a, b; Cooke and Simmons, 2000; Sillitoe, 2000). In these systems, calc-alkaline magmas are associated with hydrous, oxidizing conditions favorable for concentration, through fractional crystallization, and transport of gold (e.g., Moss et al., 2001).

The magmatic evolution of the host sequence of the LaRonde Penna deposit also may have contributed to the evolution of the hydrothermal system, including the enrichment of Au (Dubé et al., 2007). In the late, calc-alkaline intrusive phases of the Mooshla synvolcanic pluton, west of LaRonde Penna (see Mercier-Langevin et al., 2007b; Fig. 1), there are numerous veins and abundant miarolitic cavities containing auriferous sulfides and amphiboles (Galley and Lafrance, 2007). The late intrusive phases of the Mooshla are interpreted as volatile-rich magmatic pulses, thought to be responsible for the formation of the Doyon mine ore zones and aluminous alteration (Galley and Lafrance, 2007). The Mooshla intrusion also could have contributed magmatic volatiles to the LaRonde Penna system higher in the stratigraphy or represent the shallow equivalent (apophyse) of a volatile-rich subvolcanic magmatic chamber at depth.

The proposed arc rifting also may have prompted large and very efficient hydrothermal convection and thereby contributed to the formation of the larger deposits in the Doyon-Bousquet-LaRonde camp. In addition, the apparent association with the early stages of rifting of locally thickened arc crust is similar to the tectonic settings of many younger Au-rich VMS, including on the modern sea floor (e.g., Hannington et al., 1999).

## Summary and Conclusions

The LaRonde Penna deposit and the other Au-rich sulfide lenses of the Doyon-Bousquet-LaRonde mining camp are

associated with transitional to calc-alkaline felsic flows, domes and/or cryptodomes, and shallow mafic to intermediate sills and dikes defining a series of restricted coalesced subaqueous effusive centers (upper member of the Bousquet Formation). The felsic units form the upper part of a volcanic sequence composed of tholeiitic mafic to intermediate rocks (Hébécourt Formation) overlain by intermediate, tholeiitic to transitional rocks (lower member of the Bousquet Formation), which belong to a laterally extensive submarine stratum on which the upper member was emplaced. This sequence forms a continuous, differentiated volcanic succession that contrasts with the bimodal volcanic sequence of the Noranda Volcanic Complex in central Blake River Group west of the Doyon-Bousquet-LaRonde mining camp. It is, however, compatible with the inferred geodynamic setting for the Val-d'Or Formation of the Malartic Group east of the Blake River Group.

Mafic to intermediate and tholeiitic to transitional rocks of the Bousquet Formation are characterized by a low $Zr/TiO_2$ ratio, moderately enriched chondrite-normalized LREE and MREE patterns, flat HREE patterns, and pronounced negative Nb, Ta, Zr, and Hf anomalies. Felsic transitional to calc-alkaline rocks of the upper member of the Bousquet Formation are characterized by a moderate $Zr/TiO_2$ ratio, high incompatible element contents, LREE-enriched patterns, flat HREE patterns, pronounced negative Nb, Ta, and Ti anomalies, and positive Zr and Hf anomalies. The geochemical signature of the felsic rocks is similar to that of younger, ensialic arc–back-arc settings such as in the Skellefte district in Sweden. However, Nd isotope signatures of the LaRonde Penna host rocks suggest that they were generated by partial melting of depleted upper mantle and/or partial melting of juvenile material (mafic crust) with fractionated crystallization, or by a combination of those two processes. The petrogenetic evolution of the lavas may be due to the progression from depleted upper mantle diapirism associated with mafic-ultramafic magma underplating and assimilation, to magmatic differentiation (assimilation- fractional crystallization) at mid-crustal levels in subsidiary magma chambers within a ca. 2721 Ma, relatively thick, juvenile or immature mafic ± felsic back-arc crust. This geodynamic context is thought to be favorable for the generation of and sustaining long-lived, deeply seated hydrothermal fluid circulation, with possible variable contributions to the hydrothermal solutions from the metasomatized upper mantle, the crust, and high-level degassing magma chambers.

The ore lenses of the Archean LaRonde Penna Au-rich VMS deposit are associated with HREE-depleted transitional to calc-alkaline dacite, rhyodacite, and rhyolite (FII- ±FI-type). These rocks traditionally have been considered to be of limited prospectivity. This study suggests that the Archean FII-type felsic rocks and the inferred geodynamic setting in which they are produced (i.e., high-pressure felsic volcanic rocks in a rifted, back-arc setting over a relatively thick juvenile arc–back-arc lithosphere) could be related to the elevated Au content of the associated VMS deposits and therefore represent favorable exploration targets for such deposits.

## Acknowledgments

The authors wish to acknowledge the contributions of the geologists of the Geological Survey of Canada and the Ministère des Ressources naturelles et de la Faune du Québec involved in the metallogenic synthesis of the Doyon-Bousquet-LaRonde mining camp. We also thank Agnico-Eagle Mines Ltd. and the LaRonde Penna mine geology department staff for financial and logistical support and for essential scientific contributions, critical review, and authorization to publish. We greatly benefited from constructive comments on petrogenesis from A. G. Galley, H. K. Poulsen, and J. Moorhead. ICP analyses conducted at the INRS were performed by R. Gosselin. The Nd isotope analyses were carried by B. Cousens of Carleton University in Ottawa. The first author (P. Mercier-Langevin) would like to acknowledge the SEG Canada Foundation, NSERC, NRCan, INRS-ETE and FCAR-NATEQ for providing grant scholarships. Thanks are given to I. R. Jonasson and V. Bécu for their constructive comments on previous versions of the manuscript and to C.T. Barrie, S. Scott, and K. Kelley for careful reviews.

## REFERENCES

Allen, R.L., Weihed, P., and Svenson, S.-A., 1996, Setting of Zn-Cu-Au-Ag massive sulfide deposits in the evolution and facies architecture of a 1.9 Ga marine volcanic arc, Skellefte district, Sweden: Economic Geology, v. 91, p. 1022–1053.

Ayer, J., Amelin, Y., Corfu, F., Kamo, S., Ketchum, J., Kwok, K., and Trowell, N., 2002, Evolution of the southern Abitibi greenstone belt based on U-Pb geochronology: Autochtonous volcanic construction followed by plutonism, regional deformation and sedimentation: Precambrian Research, v. 115, p. 63–95.

Baragar, W.R.A., 1968, Major-element geochemistry of the Noranda volcanic belt, Quebec-Ontario: Canadian Journal of Earth Sciences, v. 5, p. 773–790.

Barrett, T.J., and MacLean, W.H., 1994, Chemostratigraphy and hydrothermal alteration in exploration for VHMS deposits in greenstones and younger volcanic rocks: Geological Association of Canada, Mineral Deposits Division, Short Course Notes, v. 11, p. 433–467.

Barrie, C.T., Ludden, J.N., and Green, T.H., 1993, Geochemistry of volcanic rocks associated with Cu-Zn and Ni-Cu deposits in the Abitibi subprovince: Economic Geology, v. 88, p. 1341–1358.

Barrie, C.T., Cousens, B.L., Hannington, M.D., Bleeker, W., and Gibson, H.L., 1999, Lead and neodymium isotope systematics of the Kidd Creek mine stratigraphic sequence and ore, Abitibi subprovince, Canada: Economic Geology Monograph 10, p. 497–510.

Bergman Weihed, J., Bergstrom, U., Billstrom, K., and Weihed, P., 1996, Geology, tectonic setting, and origin of the Paleoproterozoic Boliden Au-Cu-As deposit, Skellefte district, northern Sweden: Economic Geology, v. 91, p. 1073–1097.

Billstrom, K., and Weihed, P., 1996, Age and provenance of host rocks and ores in the Paleoproterozoic Skellefte district, northern Sweden: Economic Geology, v. 91, p. 1054–1072.

Capdevila, R., Goodwin, A.M., Ujike, O., and Gorton, M.P., 1982, Trace-element geochemistry of Archean volcanic rocks and crustal growth in southwestern Abitibi belt, Canada: Geology, v. 10, p. 418–422.

Cooke, D.R., and Simmons, S.F., 2000, Characteristics and genesis of epithermal gold deposits: Reviews in Economic Geology, v. 13, p. 221–244.

DePaolo, D.J., 1981, Trace element and isotopic effects of combined wallrock assimilation and fractional crystallisation: Earth and Planetary Science Letters, v. 53, p. 189–202.

Dimroth, E., Imreh, L., Rocheleau, M., and Goulet, N., 1982, Evolution of the south-central part of the Archean Abitibi belt, Quebec. Part I: Stratigraphy and paleogeographic model: Canadian Journal of Earth Sciences, v. 19, p. 1729–1758.

Dimroth, E., Imreh, L., Goulet, N., and Rocheleau, M., 1983a, Evolution of the south-central part of the Archean Abitibi belt, Quebec. Part II: Tectonic evolution and geomechanical model: Canadian Journal of Earth Sciences, v. 20, p. 1355–1373.

——1983b, Evolution of the south-central part of the Archean Abitibi belt, Quebec. Part III: Plutonic and metamorphic evolution and geotectonic model: Canadian Journal of Earth Sciences, v. 20, p. 1374–1388.

Dubé, B., Mercier-Langevin, P., Hannington, M.D., Lafrance, B., Gosselin, P., and Gosselin, G., 2007, The LaRonde Penna world-class Au-rich volcanogenic massive sulfide deposit, Abitibi, Québec: Mineralogy and geochemistry of alteration and implications for genesis and exploration: Economic Geology, v. 102, p. 633–666.

Franklin, J.M., Lydon, J.W., and Sangster, D.F., 1981, Volcanic-associated massive sulfide deposits: Economic Geology 75th Anniversary Volume, p. 485–627.

Franklin, J.M., Gibson, H.L., Jonasson, I.R., and Galley, A.G., 2005, Volcanogenic massive sulfide deposits: Economic Geology 100th Anniversary Volume, p. 523–560.

Fytikas, M., Innocenti, F., Kolios, N., Manetti, P., Mazzuoli, R., Poli, G., Rita, F., and Villari, L., 1986, Volcanology and petrology of volcanic products from the island of Milos and neighboring islets: Journal of Volcanology and Geothermal Research, v. 28, p. 297–317.

Galley, A.G., and Lafrance, B., 2007, Évolution et métallogénie du pluton de Mooshla: Ministère des Ressources naturelles et de la Faune, ET 2007–02, 31 p.

Gariépy, C., Dupré, B., and Allègre, C.J., 1982, Lead isotopic composition in K-feldspars from the Abitibi greenstone belt, and the genesis of the Archean crust: EOS, Transactions of the American Geophysical Union, v. 63, p. 367.

Gélinas, L., and Ludden, J.N., 1984, Rhyolitic volcanism and the geochemical evolution of an Archaean central ring complex: the Blake River Group volcanics of the southern Abitibi belt, Superior province: Physics of the Earth and Planetary Interiors, v. 35, p. 77–88.

Gélinas, L., Trudel, P., and Hubert, C., 1984, Chemostratigraphic division of the Blake River Group, Rouyn-Noranda area, Abitibi, Quebec: Canadian Journal of Earth Sciences, v. 21, p. 220–231.

Goldstein, S.L., O'Nions, R.K., and Hamilton, P.J., 1984, A Sm-Nd study of atmospheric dusts and particulates from major river systems: Earth and Planetary Science Letters, v. 70, p. 221–236.

Goodwin, A.M., 1982, Archean volcanoes in southwestern Abitibi belt, Ontario and Quebec: Form, composition, and development: Canadian Journal of Earth Sciences, v. 19, p. 1140–1155.

Gorton, M.P., and Schandl, E.S., 2000, From continents to island-arcs: A geochemical index of tectonic setting for arc-related and within-plate felsic to intermediate volcanic rocks: Canadian Mineralogist, v. 38, p. 1065–1073.

Hannington, M.D., de Ronde, C.E.J., and Petersen, S., 2005, Sea-floor tectonics and submarine hydrothermal systems: Economic Geology 100th Anniversary Volume, p. 111–141.

Hannington, M.D., Poulsen, H.K., Thompson, J.F.H, and Sillitoe, R.H, 1999, Volcanogenic gold in the massive sulfide environment: Reviews in Economic Geology, v. 8, p. 325–356.

Hart, T.R., Gibson, H.L., and Lesher, C.M., 2004, Trace element geochemistry and petrogenesis of felsic volcanic rocks associated with volcanogenic massive Cu-Zn-Pb sulfide deposits: Economic Geology, v. 99, p. 1003–1013.

Hildreth, W., 1983, The compositionally zoned eruption of 1912 in the Valley of Ten Thousand Smokes, Katmai National Park, Alaska: Journal of Volcanology and Geothermal Research, v. 18, p. 1–56.

Hochstaeder, A.G., Gill, J.B., and Morris, J.D., 1990, Volcanism in the Sumisu rift, II. Subduction and non-subduction related components: Earth and Planetary Science Letters, v. 100, p. 195–209.

Huijsmans, J.P.P., Barton, M., and Salters, V.J.M., 1988, Geochemistry and evolution of the calc-alkaline volcanic complex of Santorini, Aegean Sea, Greece: Journal of Volcanology and Geothermal Research, v. 34, p. 283–306.

Huston, D.L., 2000, Gold in volcanic-hosted massive sulfide deposits: Distribution, genesis, and exploration: Reviews in Economic Geology, v. 13, p. 400–426.

Irvine, T.N., and Baragar, W.R.A., 1971, A guide to chemical classification of the common volcanic rocks: Canadian Journal of Earth Sciences, v. 8, p. 523–548.

Ishikawa, Y., Sawaguchi, T., Iwaya, S., and Horiuchi, M., 1976, Delineation of prospecting targets for Kuroko deposits based on modes of volcanism of underlying dacite and alteration haloes: Mining Geology, v. 26, p. 105–117.

Jensen, L.S., 1985, Stratigraphy and petrogenesis of Archean metavolcanic sequences, southwestern Abitibi subprovince, Ontario: Geological Association of Canada Special Paper 28, p. 65–88.

Kerr, D.J., and Gibson, H.L., 1993, A comparison of the Horne volcanogenic massive sulfide deposit and intracauldron deposits of the Main Sequence, Noranda, Quebec: Economic Geology, v. 88, p. 1419–1442.

Laflèche, M.R., Dupuy, C., and Bourgault, H., 1992a, Geochemistry and petrogenesis of Archean mafic volcanic rocks of the southern Abitibi belt, Québec: Precambrian Research, v. 57, p. 207–241.

Laflèche, M.R., Dupuy, C., and Dostal, J., 1992b, Tholeiitic volcanic rocks of the late Archean Blake River Group, southern Abitibi greenstone belt: Origin and geodynamic implications: Canadian Journal of Earth Sciences, v. 29, p. 1448–1458.

Lafrance, B., Moorhead, J., and Davis, D., 2003a, Cadre géologique du camp minier de Doyon-Bousquet-LaRonde: Ministère des Ressources naturelles, de la Faune et des Parcs du Québec, ET 2002–07, 43 p.

Lafrance, B., Mercier-Langevin, P., Dubé, B., Galley, A.G., Hannington, M.D., Davis, D.W., Moorhead, J., Pilote, P., and Mueller, W.U., 2003b, Carte synthèse de la Formation de Bousquet: Partie ouest: Ministère des Ressources naturelles, de la Faune et des Parcs, DV 2003–08, scale 1:20,000.

Lafrance, B., Davis, D.W., Goutier, J., Moorhead, J., Pilote, P., Mercier-Langevin, P., Dubé, B., Galley, A., and Mueller, W.U., 2005, Nouvelles datations isotopiques dans la portion québécoise du Groupe de Blake River et des unités adjacentes: Ministère des Ressources naturelles et de la Faune, RP 2005–01, 15 p.

Large, R.R., 1992, Australian volcanic-hosted massive sulfide deposits: Features, styles, and genetic models: Economic Geology, v. 87, p. 471–510.

Large, R.R., Gemmel, J.B., Paulick, H., and Huston, D.L., 2001, The alteration Box Plot: A simple approach to understanding the relationship between alteration, mineralogy and lithogeochemistry associated with volcanic-hosted massive sulfide deposits: Economic Geology, v. 96, p. 957–972.

Lentz, D.R., 1998, Petrogenetic evolution of felsic volcanic sequences associated with Phanerozoic volcanic-hosted massive sulfide systems: The role of extension geodynamics: Ore Geology Reviews, v. 12, p. 289–327.

——1999, Petrology, geochemistry, and oxygen isotope interpretation of felsic volcanic and related rocks hosting the Brunswick 6 and 12 massive sulfide deposits (Brunswick belt), Bathurst mining camp, New Brunswick, Canada: Economic Geology, v. 94, p. 57–86.

Leo, G.W., Hedge, C.E., and Marvin, R.F., 1980, Geochemistry, strontium isotope data, and potassium-argon ages of the andesite-rhyolite association in the Padang area, west Sumatra: Journal of Volcanology and Geothermal Research, v. 7, p. 139–156.

Lesher, C.M., Goodwin, A.M., Campbell, I.H., and Gorton, M.P., 1986, Trace-element geochemistry of ore-associated and barren, felsic metavolcanic rocks in the Superior province, Canada: Canadian Journal of Earth Sciences, v. 23, p. 222–237.

Ludwig, K.R., 2001, *Isoplot*—geochronological toolkit for Microsoft Excel: Berkeley Geochronology Center Special Publication 1a, 55 p.

Lydon, J.W., 1988, Volcanogenic massive sulfide deposits. Part 2. Genetic models: Geoscience Canada, v. 15, p. 43–66.

McDonough, W.F., and Sun, S.S., 1995, The composition of the earth: Chemical Geology, v. 120, p. 223–253.

Mercier-Langevin, P., 2005, Géologie du gisement de sulfures massifs volcanogènes aurifères LaRonde, Abitibi, Québec: Unpublished Ph.D. thesis, Québec, Institut national de la recherche scientifique, Eau, Terre et Environnement, 694 p.

Mercier-Langevin, P., Dubé, B., Hannington, M.D., Davis, D.W., Lafrance, B., and Gosselin, G., 2007a, The LaRonde Penna Au-rich volcanogenic massive sulfide deposit, Abitibi greenstone belt, Quebec: Part I. Geology and geochronology: Economic Geology, v. 102, p. 585–609.

Mercier-Langevin, P., Dubé, B., Lafrance, B., Hannington, M.D., Galley, A., and Moorhead, J., 2007b, A group of papers devoted to the LaRonde Penna Au-rich volcanogenic massive sulfide deposit, eastern Blake River Group, Abitibi greenstone belt, Quebec—Preface: Economic Geology, v. 102, p. 577–583.

Moss, R., Scott, S.D., and Binns, R.A., 2001, Gold content of Eastern Manus basin volcanic rocks: Implications for enrichment in associated hydrothermal precipitates: Economic Geology, v. 96, p. 91–107.

Mueller, W.U., and Mortensen, J.K., 2002, Age constraints and characteristics of subacqueous volcanic construction, the Archean Hunter Mine Group, Abitibi greenstone belt: Precambrian Research, v. 115, p. 119–152.

Nelson, B.K., and DePaolo, D.J., 1984, 1700 Myr greenstone volcanic successions in southwestern North America and isotopic evolution of Proterozoic mantle: Nature, v. 312, p. 143–146.

Nohda, S., and Wasserburg, G.J., 1981, Nd and Sr isotopic study of volcanic rocks from Japan: Earth and Planetary Science Letters, v. 52, p. 264–276.

Pearce, J.A., Harris, N.B.W., and Tindle, A.G., 1984, Trace element discrimination diagrams for the tectonic interpretation of granitic rocks: Journal of Petrology, v. 25, p. 956–983.

Prior, G.J., Gibson, H.L., Watkinson, D.H., Cook, R.E., and Hannington, M.D., 1999a, Rare earth and high field strength element geochemistry of the Kidd Creek rhyolites, Abitibi greenstone belt, Canada: Evidence for Archean felsic volcanism and volcanogenic massive sulfide ore formation in a Iceland-style rift environment: Economic Geology Monograph 10, p. 457–484.

Prior, G.J., Gibson, H.L., Watkinson, D.H., Cousens, B.L., Cook, R.E., and Barrie, C.T., 1999b, Sm-Nd isotope study of rhyolites from the Kidd Creek mine area, Abitibi subprovince, Canada: Economic Geology Monograph 10, p. 485–496.

Richard, P., Shimizu, N., and Allègre, C.J., 1976, $^{143}Nd/^{146}Nd$, a natural tracer: An application to oceanic basalts: Earth and Planetary Science Letters, v. 31, p. 269–278.

Rogers, N., van Staal, C.R., McNicoll, V., and Thériault, R., 2003, Volcanology and tectonic setting of the Northern Bathurst mining camp: Part I. Extension and rifting of the Popelogan arc: Economic Geology Monograph 11, p. 157–179.

Sawkins, F.J., 1990, Integrated tectonic-genetic model for volcanic-hosted massive sulfide deposits: Geology, v. 18, p. 1061–1064.

Scott, C.R., Mueller, W.U., and Pilote, P., 2002, Physical volcanology, stratigraphy, and lithogeochimistry of an Archean volcanic arc: Evolution from plume-related volcanism to arc rifting of SE Abitibi greenstone belt, Val-d'Or, Canada: Precambrian Research, v. 115, p. 223–260.

Sillitoe, R.H., 2000, Gold-rich porphyry deposits: Descriptive and genetic models and their role in exploration and discovery: Reviews in Economic Geology, v. 13, p. 315–345.

Sillitoe, R.H., 1993a, Epithermal models: Genetic types, geometrical controls and shallow: Geological Association of Canada Special Paper 40, p. 403–417.

——1993b, Gold-rich porphyry copper deposits: Geological model and exploration implications: Geological Association of Canada Special Paper 40, p. 465–478.

Sillitoe, R.H., Hannington, M.D., and Thompson, J.F.H, 1996, High-sulfidation deposits in the volcanogenic massive sulfide environment: Economic Geology, v. 91, p. 204–212.

Smith, I.E.M., 1980, Geochemical evolution in the Blake River Group, Abitibi greenstone belt, Superior province: Canadian Journal of Earth Sciences, v. 17, p. 1292–1299.

Stern, R.A., Percival, J.A., and Mortensen, J.K., 1994, Geochemical evolution of the Minto Block: A 2.7 Ga continental magmatic arc built on the Superior proto-craton: Precambrian Research, v. 65, p.115–153.

Stone, W.E., 1990, Archean volcanism and sedimentation in the Bousquet gold district, Abitibi greenstone belt, Quebec: Implications for stratigraphy and gold concentration: Geological Society of America Bulletin, v. 102, p. 147–158.

Ujike, O., and Goodwin, A.M., 1987, Geochemistry and origin of Archean felsic metavolcanic rocks, central Noranda area, Quebec, Canada: Canadian Journal of Earth Sciences, v. 24, p. 2551–2567.

Urabe, T., 1987, Kuroko deposits modeling based on magmatic hydrothermal theory: Mining Geology, v. 37, p. 159–176.

Vervoot, J.D., White, W.M., and Thorpe, R.I., 1994, Nd and Pb isotope ratios of the Abitibi greenstone belt: New evidence for very early differentiation of the Earth: Earth and Planetary Science Letters, v. 128, p. 215–229.

Weihed, P., Bergman, J., and Bergstrom, U., 1992, Metallogeny and tectonic evolution of the Early Proterozoic Skellefte district, northern Sweden: Precambrian Research, v. 58, p. 143–167.

Wilson, M., 1989, Igneous petrogenesis: A global tectonic approach: London, Unwyn Hyman, 466 p.

Winchester, J.A., and Floyd, P.A., 1977, Geochemical discrimination of different magma series and their differentiation products using immobile elements: Chemical Geology, v. 20, p. 325–343.

Wyman, D.A., 1999, A 2.7 Ga depleted tholeiite suite: Evidence for plume-arc interaction in the Abitibi greenstone belt, Canada: Precambrian Research, v. 97, p. 27–42.

Wyman, D.A., Kerrich, R., and Polat, A., 2002, Assembly of Archean cratonic mantle lithosphere and crust: plume-arc interaction in the Abitibi-Wawa subduction-accretion complex: Precambrian Research, v. 115, p. 37–62.

Yang, K., and Scott, S.D., 2003, Geochemical relationships of felsic magmas to ore metals in massive sulfide deposits of the Bathurst mining camp, Iberian Pyrite Belt, Hokuroku district, and the Abitibi belt: Economic Geology Monograph 11, p. 457–478.

York, D., 1969, Least-square fitting of a straight line with correlated errors: Earth and Planetary Science Letters, v. 5, p. 320–324.

## APPENDIX 1

### Analytical Techniques

*Majors, traces, and REE*

Samples were crushed in a steel jaw crusher followed by milling in agate, cleaning with quartz between each sample. Major oxides were determined by inductively coupled plasma-atomic emission spectrometry (ICP-AES, Perkin Elmer Optima 3000) at the Institut national de la recherche scientifique, Centre Eau, Terre et Environnement (INRS-ETE) in Quebec City. Total S was determined using LECO combustion and infrared detection, and carbon dioxide ($CO_2$) content was measured by coulometry.

Trace elements Cs, Hf, Nb, Rb, Sr, Ta, Th, and U and rare earth elements (La, Ce, Pr, Nd, Sm, Eu, Gd, Tb, Dy, Ho, Er, Tm, Yb, and Lu), were determined by inductively coupled plasma-mass spectrometry (ICP-MS, Fison Instrument Plasmaquad II), following dissolution by lithium metaborate fusion. Trace elements Ba, Be, Cd, Cr, Co, K, Ni, Pb, Sc, V, Y, and Zr were determined by inductively coupled plasma-atomic emission spectrometry (ICP-AES) at XRAL Laboratories in Toronto, following near-total, high-temperature multiacid ($HCl$-$HNO_3$-$HF$-$HCLO_4$) digestion of 0.3-g samples.

*Sm and Nd isotope determinations*

Between 100 and 200 mg of rock powder were spiked with a mixed $^{148}Nd$-$^{149}Sm$ spike. This mixture was dissolved in 50 percent $HNO_3$-$HF$, then further attacked with $HNO_3$, and finally in HCl until no residue was visible. Samples were then taken to dryness and the residue taken up in 0.26*N* HCl and loaded onto a 10-ml borosilicate glass chromatographic column containing a 2-cm-high bed of Teflon powder coated with HDEHP (di (2-ethylhexyl) orthophosphoric acid; Richard et al., 1976). Nd was eluted using 0.26*N* HCl, followed by Sm in 0.5*N* HCl. Total procedure blanks for Nd were <400 pg. Concentrations were precise to ±1 percent, but $^{147}Sm/^{144}Nd$ are reproducible to 0.5 percent. Samples were loaded with 0.3*N* $H_3PO_4$ on one side of a Re double filament and run at temperatures of 1,800° to 1,850°C in a Finnigan MAT261 multicollector mass spectrometer at Carleton University, Ottawa (B. Cousens). Isotopic ratios were normalized to $^{146}Nd/^{144}Nd = 0.7219$. Precision based on analysis of duplicate samples and standards was ±0.8 epsilon units. Analyses of U.S.G.S. standard BCR-1 yielded Nd = 29.02 ppm, Sm = 6.68 ppm, and $^{143}Nd/^{144}Nd = 0.512668 \pm 0.000020$ ($n = 4$). Over 70 runs of the La Jolla standard (September 1992-February 2002) average $^{143}Nd/^{144}Nd = 0.511876 \pm 0.000018$.

**APPEN**

Geochemistry of Least Altered Felsic Volcanic Rocks

| | Dacite-rhyodacite, subunit 5.1b-(d) | | | | | | | | | | | | | | Rhyodacite-dac | |
|---|---|---|---|---|---|---|---|---|---|---|---|---|---|---|---|---|
| | BD-028-2000 | BD-029-2000 | BD-186-2000 | BD-306-2000 | PL-028-2000 | PL-074-2000 | BD-216-2001 | BD-218-2001 | BD-419-2001 | BD-421-2001 | PL-072-2001 | PL-073-2001 | PL-165-2001 | PL-180-2001 | BD-495-2000 | BD-498-2000 |
| $SiO_2$ (%) | 67.40 | 72.60 | 72.11 | 73.30 | 71.70 | 77.34 | 69.60 | 70.31 | 72.69 | 74.10 | 69.36 | 71.16 | 72.48 | 73.67 | 69.60 | 71.40 |
| $TiO_2$ | 0.67 | 0.59 | 0.66 | 0.59 | 0.69 | 0.67 | 0.68 | 0.76 | 0.59 | 0.55 | 0.62 | 0.72 | 0.65 | 0.47 | 0.71 | 0.68 |
| $Al_2O_3$ | 16.10 | 14.10 | 14.83 | 14.10 | 15.90 | 11.76 | 15.50 | 16.99 | 13.82 | 13.68 | 14.79 | 14.38 | 14.96 | 13.64 | 14.80 | 13.61 |
| $Fe_2O_3t$ | 3.10 | 1.87 | 0.63 | 0.73 | 0.56 | 0.89 | 2.46 | 0.64 | 0.55 | 0.80 | 2.87 | 2.38 | 1.05 | 1.67 | 3.49 | 3.91 |
| MnO | 0.06 | 0.03 | 0.01 | 0.01 | 0.01 | 0.03 | 0.05 | 0.01 | 0.01 | 0.02 | 0.07 | 0.08 | 0.03 | 0.03 | 0.10 | 0.11 |
| MgO | 1.05 | 0.74 | 0.22 | 0.29 | 0.33 | 0.11 | 0.79 | 0.32 | 0.17 | 0.30 | 0.79 | 0.59 | 0.30 | 0.37 | 0.90 | 0.70 |
| CaO | 2.15 | 1.77 | 1.97 | 1.69 | 1.23 | 1.02 | 1.65 | 1.11 | 2.21 | 1.31 | 1.78 | 2.18 | 0.94 | 2.00 | 1.61 | 1.74 |
| $Na_2O$ | 5.96 | 6.70 | 5.67 | 6.53 | 6.08 | 5.22 | 6.96 | 5.93 | 5.51 | 5.29 | 6.24 | 4.77 | 5.81 | 5.04 | 5.99 | 4.17 |
| $K_2O$ | 1.69 | 0.39 | 1.55 | 0.89 | 1.73 | 0.82 | 0.86 | 2.75 | 1.08 | 1.64 | 1.20 | 1.72 | 1.61 | 1.08 | 1.69 | 2.80 |
| $P_2O_5$ | 0.16 | 0.14 | 0.14 | 0.14 | 0.17 | 0.20 | 0.21 | 0.14 | 0.01 | 0.14 | 0.16 | 0.14 | 0.18 | 0.10 | 0.15 | 0.13 |
| LOI | 0.95 | 0.35 | 1.37 | 0.85 | 0.85 | 0.64 | 0.57 | 0.96 | 1.27 | 0.91 | 0.62 | 0.99 | 0.80 | 0.55 | 0.30 | 0.74 |
| Total | 99.29 | 99.28 | 99.16 | 99.11 | 99.25 | 98.71 | 99.58 | 100.08 | 98.06 | 98.88 | 98.62 | 99.25 | 98.91 | 98.75 | 99.34 | 99.98 |
| S | 0.03 | 0.13 | 0.17 | 0.13 | 0.06 | 0.04 | 0.17 | 0.02 | 0.07 | 0.06 | 0.01 | 0.04 | 0.01 | 0.02 | 0.06 | 0.28 |
| $CO_2$ | 0.27 | 0.11 | 0.70 | 0.65 | 0.32 | 0.25 | 0.19 | 0.13 | 1.03 | 0.42 | 0.34 | 0.45 | 0.06 | 0.12 | 0.07 | 0.08 |
| FeO[1] | 2.79 | 1.68 | 0.57 | 0.66 | 0.50 | 0.80 | 2.21 | 0.58 | 0.49 | 0.72 | 2.58 | 2.14 | 0.94 | 1.50 | 3.14 | 3.51 |
| Y (ppm) | 35.0 | 27.0 | 23.6 | 17.0 | 23.0 | 29.8 | 28.4 | 26.7 | 13.1 | 27.5 | 31.2 | 37.0 | 28.3 | 31.9 | 40.0 | 38.8 |
| Zr | 205.0 | 172.0 | 164.4 | 156.0 | 184.0 | 179.1 | 171.4 | 201.8 | 155.3 | 173.9 | 180.3 | 205.5 | 168.9 | 217.2 | 197.0 | 198.2 |
| Ba | 441 | 59 | 446 | 301 | 469 | 322 | 193 | 817 | 324 | 381 | 521 | 374 | 486 | 378 | 413 | 536 |
| V | 56 | 50 | 64 | 49 | 94 | 26 | 64 | 104 | 53 | 48 | 52 | 16 | 61 | 38 | 15 | 13 |
| Sc | 10.7 | 9.7 | 10.0 | 7.0 | 14.1 | 13.0 | 10.4 | 17.2 | 6.6 | 6.5 | 9.7 | 14.4 | 10.3 | 6.8 | 13.1 | 12.5 |
| Be | 1.00 | 1.00 | 0.70 | 0.60 | 0.70 | 1.60 | 0.92 | 1.00 | 0.83 | 0.92 | 1.10 | 0.83 | 0.70 | 1.20 | 0.90 | 1.00 |
| Cr | 2 | 3 | 2 | 1 | 5 | 25 | 24 | 6 | 16 | 17 | 2 | 1 | 2 | 2 | 2 | 3 |
| Co | 14 | 10 | 8 | 14 | 5 | 1.5 | 10 | 6 | 7 | 4 | 10 | 11 | 9 | 8 | 8 | 1 |
| Ni | 5 | 3 | 8 | 11 | 4 | 3.5 | 7 | 7 | 11 | 6 | 2 | 3 | 2 | 2 | 3 | 2 |
| K | 1.35 | 0.29 | 1.23 | 0.68 | 1.46 | 0.73 | 0.67 | 1.96 | 0.89 | 1.25 | 1.11 | 1.47 | 1.32 | 0.92 | 1.43 | 2.29 |
| Ti[(1)] | 4041 | 3531 | 3932 | 3531 | 4143 | 4021 | 4057 | 4564 | 3533 | 3324 | 3697 | 4338 | 3889 | 2838 | 4238 | 4089 |
| Sr | 189 | 203 | 150 | 158 | 120 | 168 | 184 | 148 | 168 | 141 | 271 | 168 | 114 | 339 | 89 | 165 |
| Cd | 0.5 | 0.5 | 1.0 | 0.5 | 1.0 | 1.0 | 0.5 | 0.5 | 0.5 | 0.5 | 0.5 | 0.5 | 0.5 | 0.5 | 0.5 | 1.0 |
| Rb | | | 33.41 | | | 19.30 | | | 23.73 | | | | | | | 43.24 |
| Nb | | | 8.55 | | | 10.60 | | | 8.54 | | | | | | | 10.42 |
| Cs | | | 1.44 | | | 0.40 | | | 0.78 | | | | | | | 1.47 |
| Hf | | | 3.85 | | | 4.40 | | | 3.62 | | | | | | | 4.75 |
| Ta | | | 0.46 | | | 0.62 | | | 0.46 | | | | | | | 0.57 |
| Pb | | | 7.17 | | | 0.05 | | | 4.87 | | | | | | | 8.99 |
| Th | | | 9.64 | | | 7.70 | | | 9.02 | | | | | | | 7.93 |
| U | | | 2.24 | | | 1.70 | | | 2.31 | | | | | | | 1.78 |
| REE | | | | | | | | | | | | | | | | |
| La | | | 45.52 | | | 39.30 | | | 40.33 | | | | | | | 37.74 |
| Ce | | | 93.30 | | | 86.70 | | | 82.09 | | | | | | | 79.33 |
| Pr | | | 11.11 | | | 10.60 | | | 8.44 | | | | | | | 9.91 |
| Nd | | | 38.52 | | | 40.50 | | | 29.82 | | | | | | | 36.12 |
| Sm | | | 7.52 | | | 7.40 | | | 4.87 | | | | | | | 7.86 |
| Eu | | | 1.74 | | | 1.90 | | | 1.30 | | | | | | | 1.87 |
| Gd | | | 4.89 | | | 6.60 | | | 3.24 | | | | | | | 6.05 |
| Tb | | | 0.77 | | | 0.90 | | | 0.43 | | | | | | | 1.07 |
| Dy | | | 4.41 | | | 5.10 | | | 2.73 | | | | | | | 6.44 |
| Ho | | | 0.92 | | | 1.00 | | | 0.52 | | | | | | | 1.39 |
| Er | | | 2.52 | | | 2.70 | | | 1.56 | | | | | | | 3.81 |
| Tm | | | 0.40 | | | 0.39 | | | 0.24 | | | | | | | 0.60 |
| Yb | | | 2.71 | | | 2.40 | | | 1.70 | | | | | | | 3.93 |
| Lu | | | 0.44 | | | 0.33 | | | 0.28 | | | | | | | 0.63 |

[1] Calculated from $Fe_2O_3$, assuming all iron is present as FeO; Ti calculated from $TiO_2$

**DIX 2**

of the Host Sequence of the LaRonde Penna Deposit

| ite, unit 5.2b | | Rhyolitic domes or cryptodomes, subunit 5.2b-R | | | | | | Feldspar and quartz phyric rhyolite, unit 5.3 | | | | | Upper felsic unit, unit 5.5 | | | | |
|---|---|---|---|---|---|---|---|---|---|---|---|---|---|---|---|---|---|
| BD-023-2001 | PL-2002-189 | PL-002-2000 | PL-003-2000 | PL-021-2000 | PL-039-2000 | PL-043-2000 | PL-138-2000 | BD-071-2000 | BD-110-2000 | BD-279-2000 | PL-115-2000 | PL-126-2000 | BD-058-2001 | BD-476-2001 | PL-065-2001 | PL-082-2001 | PL-083-2001 |
| 71.87 | 70.59 | 74.86 | 74.77 | 73.70 | 77.89 | 73.31 | 75.00 | 76.90 | 75.70 | 74.80 | 72.97 | 76.50 | 71.54 | 74.31 | 74.17 | 76.58 | 71.14 |
| 0.64 | 0.64 | 0.28 | 0.29 | 0.33 | 0.29 | 0.45 | 0.51 | 0.21 | 0.20 | 0.19 | 0.24 | 0.21 | 0.46 | 0.24 | 0.31 | 0.39 | 0.49 |
| 14.83 | 14.92 | 13.71 | 14.27 | 14.30 | 12.54 | 12.63 | 13.80 | 12.70 | 13.20 | 12.48 | 15.86 | 11.50 | 12.70 | 13.32 | 12.69 | 11.55 | 13.37 |
| 1.08 | 2.09 | 2.08 | 2.39 | 0.88 | 0.36 | 1.81 | 1.89 | 1.18 | 1.35 | 1.21 | 1.77 | 1.33 | 2.74 | 1.92 | 0.97 | 0.97 | 1.69 |
| 0.04 | 0.04 | 0.06 | 0.05 | 0.04 | 0.02 | 0.05 | 0.07 | 0.03 | 0.03 | 0.04 | 0.04 | 0.04 | 0.04 | 0.03 | 0.06 | 0.02 | 0.05 |
| 0.18 | 0.50 | 0.61 | 0.70 | 0.35 | 0.12 | 0.42 | 0.43 | 0.37 | 0.37 | 0.47 | 0.48 | 0.30 | 0.58 | 0.48 | 0.23 | 0.24 | 0.54 |
| 2.20 | 2.22 | 0.69 | 1.21 | 1.62 | 1.87 | 1.71 | 1.65 | 2.11 | 1.00 | 4.67 | 2.52 | 2.73 | 3.17 | 2.42 | 1.29 | 2.11 | 2.74 |
| 6.40 | 6.00 | 3.63 | 2.65 | 4.93 | 5.63 | 5.13 | 4.86 | 4.05 | 6.17 | 1.26 | 3.80 | 3.37 | 2.55 | 2.27 | 4.57 | 2.44 | 4.70 |
| 1.50 | 0.78 | 3.40 | 4.00 | 2.00 | 2.26 | 0.86 | 1.58 | 1.55 | 0.68 | 2.10 | 2.20 | 1.34 | 2.42 | 2.49 | 2.42 | 2.87 | 1.23 |
| 0.18 | 0.16 | 0.05 | 0.05 | 0.07 | 0.07 | 0.07 | 0.10 | 0.03 | 0.04 | 0.03 | 0.04 | 0.04 | 0.04 | 0.04 | 0.07 | 0.06 | 0.07 |
| 1.23 | 0.47 | 1.30 | 1.82 | 1.75 | 1.79 | 1.17 | 0.20 | 0.85 | 0.50 | 2.34 | 1.39 | 1.24 | 2.65 | 1.37 | 0.52 | 0.90 | 1.40 |
| 100.27 | 98.40 | 100.67 | 102.20 | 99.97 | 102.84 | 97.61 | 100.09 | 99.98 | 99.24 | 99.59 | 101.30 | 98.59 | 99.59 | 99.30 | 97.49 | 98.34 | 97.63 |
| 0.01 | 0.01 | 0.05 | 0.01 | 0.06 | 0.03 | 0.05 | 0.10 | 0.03 | 0.37 | 0.11 | 0.10 | 0.02 | 0.74 | 0.33 | 0.01 | 0.15 | 0.08 |
| 0.85 | 0.04 | 0.30 | 0.47 | 1.00 | 1.23 | 0.51 | 0.02 | 0.45 | 0.07 | 1.30 | 0.22 | 0.53 | 1.30 | 0.47 | 0.28 | 0.26 | 0.60 |
| 0.97 | 1.88 | 1.87 | 2.15 | 0.79 | 0.32 | 1.63 | 1.70 | 1.06 | 1.22 | 1.09 | 1.59 | 1.20 | 2.47 | 1.73 | 0.87 | 0.87 | 1.52 |
| 24.2 | 30.2 | 19.5 | 17.5 | 19.0 | 21.1 | 32.6 | 34.0 | 14.0 | 17.0 | 16.1 | 23.9 | 19.7 | 30.0 | 18.8 | 21.5 | 22.4 | 24.9 |
| 155.2 | 188.6 | 165.9 | 177.4 | 206.0 | 179.1 | 219.9 | 206.0 | 122.0 | 131.0 | 112.4 | 146.3 | 128.0 | 234.0 | 169.3 | 181.2 | 184.1 | 155.2 |
| 596 | 245 | 815 | 772 | 394 | 825 | 259 | 170 | 357 | 273 | 491 | 827 | 494 | 802 | 497 | 1290 | 575 | 689 |
| 72 | 51 | 14 | 23 | 7 | 7 | 34 | 31 | 13 | 9 | 12 | 15 | 12 | 35 | 15 | 11 | 36 | 81 |
| 9.1 | 14.2 | 3.4 | 3.9 | 3.3 | 3.4 | 6.6 | 8.7 | 2.5 | 2.5 | 2.8 | 3.0 | 3.5 | 7.4 | 3.3 | 3.6 | 4.7 | 10.4 |
| 0.92 | 1.90 | 1.20 | 1.30 | 1.40 | 0.60 | 0.90 | 0.70 | 1.30 | 1.10 | 1.30 | 1.50 | 1.70 | 1.30 | 1.30 | 0.70 | 1.00 | 1.00 |
| 2 | 4 | 3 | 4 | 1 | 2 | 2 | 3 | 1 | 0.5 | 2 | 7 | 1 | 2 | 3 | 4 | 2 | 5 |
| 8 | 3 | 1 | 3 | 1 | 1 | 2 | 3 | 3 | 2 | 2 | 2 | 1 | 8 | 4 | 3 | 7 | 12 |
| 2 | 4 | 3 | 3 | 2 | 1 | 2 | 2 | 1 | 1 | 3 | 6 | 1 | 4 | 6 | 4 | 3 | 5 |
| 1.26 | | 2.57 | 3.11 | 1.71 | 1.60 | 0.74 | 1.39 | 1.29 | 0.57 | 1.83 | 1.74 | 0.00 | 2.00 | 2.05 | 1.92 | 2.46 | 1.13 |
| 3807 | 3830 | 1679 | 1743 | 1984 | 1767 | 2710 | 3051 | 1229 | 1223 | 1116 | 1411 | 1253 | 2752 | 1445 | 1852 | 2355 | 2946 |
| 181 | 300 | 199 | 229 | 128 | 100 | 121 | 144 | 260 | 248 | 205 | 357 | 281 | 114 | 178 | 126 | 171 | 372 |
| 0.5 | 0.5 | 1.0 | 1.0 | 1.0 | 1.0 | 1.0 | 1.0 | 0.5 | 0.5 | 1.0 | 1.0 | 1.0 | 0.5 | 0.5 | 0.5 | 0.5 | 0.5 |
| 31.65 | | | | | 34.70 | 33.50 | | | | 75.52 | | 53.30 | | 69.98 | | 69.47 | |
| 7.65 | | | | | 13.27 | 10.42 | | | | 12.88 | | 12.90 | | 15.17 | | 8.37 | |
| 0.90 | | | | | 0.44 | 0.73 | | | | 1.25 | | 0.90 | | 1.74 | | 1.41 | |
| 3.61 | | | | | 3.86 | 5.05 | | | | 2.84 | | 3.10 | | 3.41 | | 4.17 | |
| 0.45 | | | | | 0.89 | 0.58 | | | | 0.96 | | 1.09 | | 0.95 | | 0.49 | |
| 6.35 | | | | | 4.43 | 7.43 | | | | 5.72 | | 2.10 | | 8.31 | | 8.05 | |
| 8.46 | | | | | 11.22 | 12.40 | | | | 11.62 | | 11.40 | | 11.95 | | 9.15 | |
| 2.22 | | | | | 2.42 | 2.88 | | | | 2.68 | | 2.70 | | 3.01 | | 2.42 | |
| 39.19 | | | | | 41.10 | 45.73 | | | | 39.86 | | 39.70 | | 44.13 | | 38.70 | |
| 85.82 | | | | | 79.39 | 90.58 | | | | 69.59 | | 74.20 | | 78.88 | | 87.24 | |
| 9.21 | | | | | 9.02 | 10.67 | | | | 7.32 | | 7.50 | | 7.95 | | 9.18 | |
| 35.62 | | | | | 29.96 | 36.35 | | | | 21.89 | | 23.00 | | 26.40 | | 34.29 | |
| 6.04 | | | | | 5.73 | 7.16 | | | | 3.52 | | 3.40 | | 4.05 | | 5.91 | |
| 1.57 | | | | | 1.30 | 1.37 | | | | 0.62 | | 0.70 | | 0.95 | | 1.30 | |
| 4.96 | | | | | 3.95 | 4.61 | | | | 2.22 | | 2.90 | | 3.21 | | 4.59 | |
| 0.63 | | | | | 0.61 | 0.82 | | | | 0.40 | | 0.40 | | 0.43 | | 0.58 | |
| 4.33 | | | | | 3.55 | 5.04 | | | | 2.44 | | 2.70 | | 2.82 | | 3.76 | |
| 0.82 | | | | | 0.73 | 1.09 | | | | 0.55 | | 0.60 | | 0.59 | | 0.76 | |
| 2.38 | | | | | 1.94 | 3.06 | | | | 1.61 | | 1.80 | | 1.88 | | 2.26 | |
| 0.36 | | | | | 0.31 | 0.50 | | | | 0.28 | | 0.30 | | 0.30 | | 0.33 | |
| 2.37 | | | | | 2.10 | 3.46 | | | | 2.04 | | 2.20 | | 2.14 | | 2.29 | |
| 0.37 | | | | | 0.34 | 0.55 | | | | 0.35 | | 0.37 | | 0.36 | | 0.37 | |